Alma Mater Studiorum – Università di Bologna

DOTTORATO DI RICERCA IN

CHIMICA

Ciclo XXXII

Settore Concorsuale: 03/A1 Chimica Analitica

Settore Scientifico Disciplinare: CHIM/01 Chimica Analitica

Luminescent biosensors for forensic applications based on new ultrasensitive Silicon Photomultiplier detector

Presentata da: Marcello D'Elia

Coordinatore Dottorato

Chiar.ma Prof.ssa Domenica Tonelli

Supervisore

Chiar.mo Prof. Aldo Roda

Co-Supervisore

Chiar.ma Prof.ssa Elisa Michelini

Esame finale anno 2020

Abstract

Global security threats have become a major worldwide concern and their early detection represents a major challenge to current monitoring technologies. The aim of this PhD research was thus focused on the development of a new portable analytical device suitable for implementation by scientific police routine screenings and inspections.

The suitability of different portable light detectors was investigated, including charge coupled devices (CCDs), smartphone integrated Complementary Metal-Oxide-Semiconductor (CMOSs) and Silicon Photomultiplier (SiPM) technology. SiPM was selected thanks to its high sensitivity combined with very low power supply (few tens of volts).

The ArduSiPM, a SiPM detector for the Arduino DUE microcontroller, was exploited to detect bioluminescence and chemiluminescence. A new portable device for low-light detection, named LuminoSiPM, was fabricated by 3D printing together with disposable sample-holders for liquid samples and origami paper-based biosensors. Several parameters were optimized to reduce dark noise and improve signal to noise ratio. A comparison of the LuminoSiPM analytical performance, in terms of delectability and wavelength sensitivity dependence, was performed with benchtop PMT instrumentation (Varioskan Flash), a cooled CCD sensor (ATIK 383L), and OnePlus 6 smartphone integrated CMOS, using two luciferases/luciferin system emitting a different wavelength: the green-emitting *P. pyralis* mutant PpyGRT (λ_{max} 550 nm) and the blue-emitting NanoLuc (λ_{max} 490 nm). A limit of detection of 5.3×10^{-9} M was obtained with Nanoluc, about one order of magnitude lower than those obtained with the ATIK 383L CCD camera. These promising results have allowed the development of portable biosensors based of this new device.

As proof-of-principle, a paper-based origami chemiluminescent enzyme biosensor for forensic application has been developed. This biosensor is based on the inhibition of acetylcholinesterase (AChE) activity by molecules, such as organophosphate pesticides and nerve agents and, combined with LuminoSiPM, showed useful for bio-chemiluminescence detections at the point-of-need in forensic investigations.

Index

Chapter 1

Introduction

Global security threats have become a major worldwide concern and their early detection represents a major challenge to current monitoring technologies (Sadik et al., 2004). The routine monitoring of water, food and environment for chemical and biological threat agents is often hampered by the complexity of available techniques that cannot be used for real-time, cost-effect and on-field routine monitoring (Fitch et al., 2003). Current techniques that are applied for scientific police routine screenings, such as gas chromatography (GC) or liquid chromatography (LC) combined with mass spectrometry (MS), tandem mass spectrometry (MS/MS), and high-resolution mass spectrometry (HRMS) approaches, require time-consuming pre-treatment processes and expert operators. Moreover, they are not suitable for rapid monitoring of illegal drugs, for example in airports, customs and decentrate settings. Therefore, sensitive, reliable, and cost-effective first-level screening methods in a biosensor format are urgently required to reduce the large number of samples to be analyzed with the conventional analytical techniques (Singh et al., 2017; green et al., 2003). The aim of the PhD research was focused on the development of on-field uses of new miniaturized and portable analytical devices to be implemented by scientific police routine screenings and inspections. The use of bioluminescence and chemiluminescence allow to develop sensitive and on the mean time simple biosensor format with wide applicability in criminal investigations and other forensic-related activities.

1.1. Light sensors for portable instruments

One of the most challenging issues for the development of portable optical biosensors for on-site analysis is the integration of the biological sensing element with a suitable light detection system. Although there are many detectors currently used and able to measure low light emission, some aspects in their intrinsic technology have to be considered when a portable device need to be developed including the power supply and the temperature dependence of the instrumental specific noise (Pires et al., 2014).

1.2 Charge coupled devices - CCD sensors

A charge coupled device (CCD) is an integrated circuit etched onto a silicon surface forming light sensitive elements called pixels (Damulira et al., 2019; Graham et al., 2013). The pixel is formed by metal-oxide-semiconductor (MOS) condenser, which interact with photons absorbing their energy. This absorption can excite an electron from the silicon's valence band to its conduction band in a process known as the photoelectric effect. Photoelectrons are then captured and stored by applying a positive voltage to the pixel to hold the electrons in a potential well. The varying number of electrons stored in each pixel produces different voltages across the pixel that is measured and the analog voltage converted to digital "counts" by an external Analog to Digital convert (ADC) circuit. Signal detection depends on the relative strengths of the signal and overall noise present on the detector. All CCDs benefit from working at lower temperatures. Thermal energy is able to excite extraneous electrons into the image pixels and these cannot be distinguished from the actual image photoelectrons. This process generates noise and is called 'dark current.'

One of the great features of the CCD camera used as light detector relies on the possibility of cooling the sensor with a Peltier chamber down to -10 °C, allowing a significant decrease of CCD dark current generated by thermal energy. It has been in fact

demonstrated that the dark-current shot noise, whose contribution is often the major source of noise, is cut approximately in half for every 6°C reduction in chip temperature (Christensen and Herron, 2009). The variation due to dark current shot noise is described by the following equation:

$$\sigma_d^2 = 2qI_d\Delta f \qquad \text{(Eq.1)}$$

where σ_d^2 = variance of shot noise, q= charge of an electron, I_d= amount of dark current, Δf = electronic bandwidth of the sensing system.

Although it requires additional components to avoid water vapour condensation on the camera window in humid environments and a larger power supply, the resulting reduction of shot noise allows to distinguish weak bioluminescent signals from the dark background signal with high reproducibility. This of course has its limits; most CCDs don't function well at temperatures lower than –120°C.

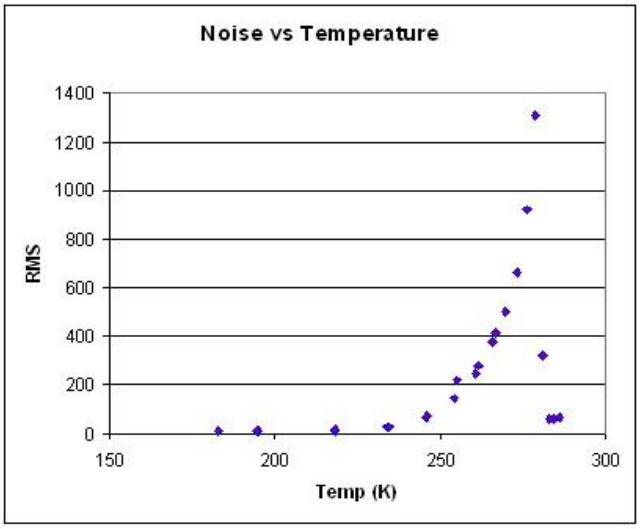

Fig n.1 - temperature effects on CCD dark current. Note that cooling to around –100°C nearly removes the noise generated by dark current (image from *http://www.specinst.com/What_Is_A_CCD.html*)

CCDs have excellent sensitivity, quantum efficiency and dynamic range but, due to the high complexity of circuits, require as much as 100 times more power than other equivalent matrix sensors (e.g. CMOS).

1.3 Complementary Metal-Oxide-Semiconductor CMOS sensors

The Complementary Metal-Oxide-Semiconductor - CMOS sensor (also known as Active Pixel Sensor - APS) differs from its technological competitor, the CCD, because have most of their required circuitry and components integrated in the sensor. Each pixel contains light sensor, an active amplifier, an analog-to-digital converter and other components for sensor functionality, resulting in a smaller and a less power consuming system. Typically, a CMOS has an integrated circuit with an array of pixel sensors; each pixel converts photoelectrons into a voltage signal, whereas, in a CCD, the electrical charge of each pixel sensor is transferred to an output node to be converted into a voltage signal by other circuits.

In the last years, thanks to the minor circuit complexity and lower power consumption, all smartphones and consumer imaging products have adopted CMOS-based technology. Therefore, thanks to this great commercial success, CMOS sensors' performances have been greatly improved, being able to compete with more sensitive CCD also for technical and scientific applications (Norian et al., 2014).

1.4 Photodiodes

In the field of low-intensity photon detection, photomultiplier tubes (PMT) are the most known and employed devices, due to their efficiency, photon sensitivity and stability. However, the PMT technology has relevant drawbacks, such as: intrinsic complexity and fragility (sealed vacuum tube); the use high voltages (typically, more than 1000 Volt). These characteristics represent a limit, in the perspective of developing a lightweight, portable and self-powered instrument. Photodiodes are semiconductor junctions, of *p*-*n* type, highly doped in an asymmetric scheme (Fig.2). Usually, the *p* zone is more doped (p+) than n zone. A

forward biased photodiode has the same characteristics of a normal diode, except for its light sensitivity. Instead, applying an inverse polarization to photodiodes, it is possible to generate a depletion region, of linear dimension. The reverse biasing of a photodiode is accomplished by setting the cathode of the detector at a higher electric potential than the anodes.

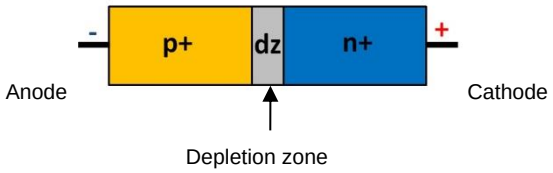

Fig.2 - Layers' scheme of a photodiode PN inversely polarized

If an electromagnetic radiation hits one side of junction with an energy, $h\nu$, greater than the jump from valence band to conduction band of material, it will form pairs of electron-hole (***e-h***). Due to the electric field applied, electrons will flow towards the ***n*** zone and holes to the ***p*** part of diode. The absence of pairs in the depletion zone produces an inverse "*photocurrent*", with a related electric signal. The main features of photodiodes are the *Quantum Efficiency* and *Responsivity*. The Quantum Efficiency is related to the pairs of "e-h" generated by each photon impacting on sensor surface; the Responsivity measures the gain in terms of photoelectrical output per radiant (photonic) input.

1.5 PIN Photodiodes

A PIN photodiode is an evolution of PN photodiodes, consisting of an intrinsic semiconductor region *"nd"* sandwiched between heavily doped p+ and n+ regions, the depletion (i.e. not doped or weakly doped) layer. Most of the photons are absorbed in the intrinsic region, and carriers generated therein can efficiently contribute to the photocurrent (Dai et al., 2019). The working principle of the PIN diode is basically the same as a normal

diode. The main difference is that the depletion region, that normally exists between both the P and N regions in a reverse biased or unbiased diode, is larger.

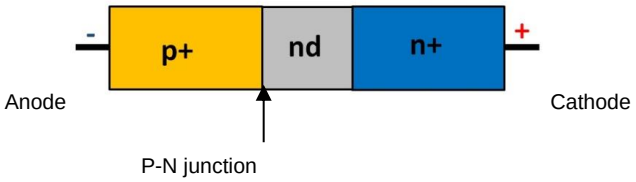

Fig.3 - Layers' scheme of inversely polarized photodiode PIN

The intrinsic layer between the p+ and n+ regions is depleted completely, because of the electric field created by the top and bottom layers. When the field strength is increased, by applying a reverse bias voltage, it produces an enlargement of the depleted zone. When a photon hits the device an electron/hole pair, due to the inner-photoelectric effect, can be created and electrons travel towards the cathode, while the holes drift to the anode. This produces a faint electrical signal.

However, depending on reverse bias voltages applied to the ends of the junction, photodiodes can work in three different regimes (Fig. 4): Photodiode (PN or PIN types) range, Avalanche (APD) range and "Geiger-APD" range (SPAD or SiPM).

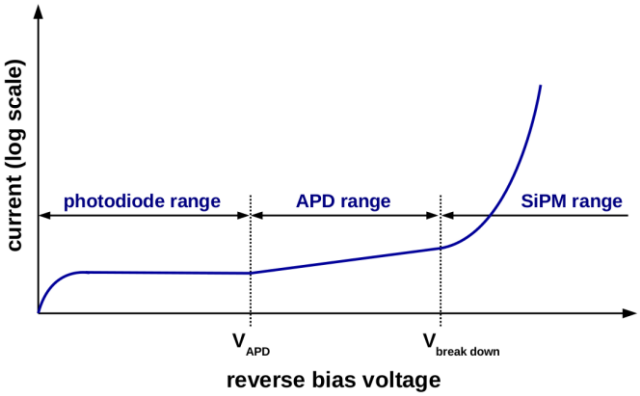

Fig.4 - Operative ranges, in terms of reverse voltage applied, of different class of sensors, PiN-APD- SiPM (G-APD), and related currents generated.

1.6 Avalanche Photodiodes (APD)

Internal gain of inversely polarized photodiodes is near null, therefore, when greater photon-sensitivity levels are requested, Avalanche Photodiodes (APD) are commonly employed (Yi et al., 2019). An APD photodiode is generally constituted by four different semiconductor layers, each of them featured by different kind and concentration of doped sites (Fig. 5):

• a zone "***p+***", rich of acceptors (acceptors number/ $cm^3 > 10^{17}$);

• a zone "***nd***" of intrinsic semiconductor, not doped, to maintain near-constant the electric field into the junctions and to lowering its capacitance;

• a zone "***p***", less rich of acceptors than the "*p+*";

• a zone "***n+***", where is high the donors' concentration (donors number/$cm^3 > 10^{17}$).

Primary charges, derived from photon impacts, flow through the "p" zone and produce, as consequence, secondary charges, which will form the photocurrent; the insertion of "p" layer is essential, in order to produce the avalanche amplification effect. APD Diodes fundamental parameters is the "*Random multiplication factor*" (*M)*, which represents the secondary pairs number *e-h* generated by each primary pair. This parameter raises with the inverse polarization, reaching typical figures of gai in the range $10^2 - 10^3$.

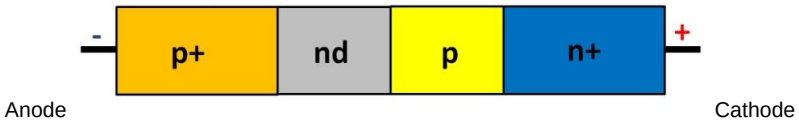

Fig.5 - Semiconductors' layer scheme of APD photodiode

However, in applications where high sensitivity is required, photodiodes PIN (gain=1) are not suitable as well as Avalanche Photo Diodes gain figures (max 1000 X) might result not sufficient.

To obtain further gain increases, it is needed to operate to bias regimes greater than the so-called “breakdown voltage” (V_{bd}); when the reverse bias voltage applied to an APD is higher than its breakdown voltage, current's behavior becomes exponential. The difference between V_{bias} and V_{bd} is called the overvoltage (V_{ov}), so

$$V_{bias} = V_{bd} + V_{ov} \qquad \text{(Eq.2)}$$

Beyond this limit, when a sufficiently high electric field (> 5 x 10^5 V/cm) is generated within the depletion region of the silicon (achieved by the sensor design and application of a recommended bias), a charge carrier created there will be accelerated to a point where kinetic energy is sufficient to create secondary charge pairs, through a process called “impact ionization”.

In this way, a single absorbed photon can trigger a self-sustaining ionization cascade, that will spread throughout the silicon volume subjected to the electric field. The silicon will break down and become conductive, effectively amplifying the original electron-hole pair into a macroscopic current flow. This process is called Geiger discharge, in analogy to the ionization discharge observed in a Geiger-Müller tube. An APD diode working in this range, is a so-called “*Geiger mode Avalanche Diode*” (G-APD) or “*Single Photon Avalanche diode*” (SPAD), whose gain increments ranging from 10^4 to 10^7. However, in order to rapidly quench discharges and avoid diodes damages, techniques of avalanches’ containment are necessary. The quenching stage is ordinary realized by resistors, which, simply developing a voltage drop on a high impedance load, lower the bias voltage of the SPAD. In these conditions, the electric field is so high that even a single charge carrier can produce a discharge (avalanche), with high level currents signal gains which can compete with PMT. While in APD only electrons contribute to the avalanche, which is self-quenched, in G-APD both electrons and holes have an active role in the avalanche (Fig. 6).

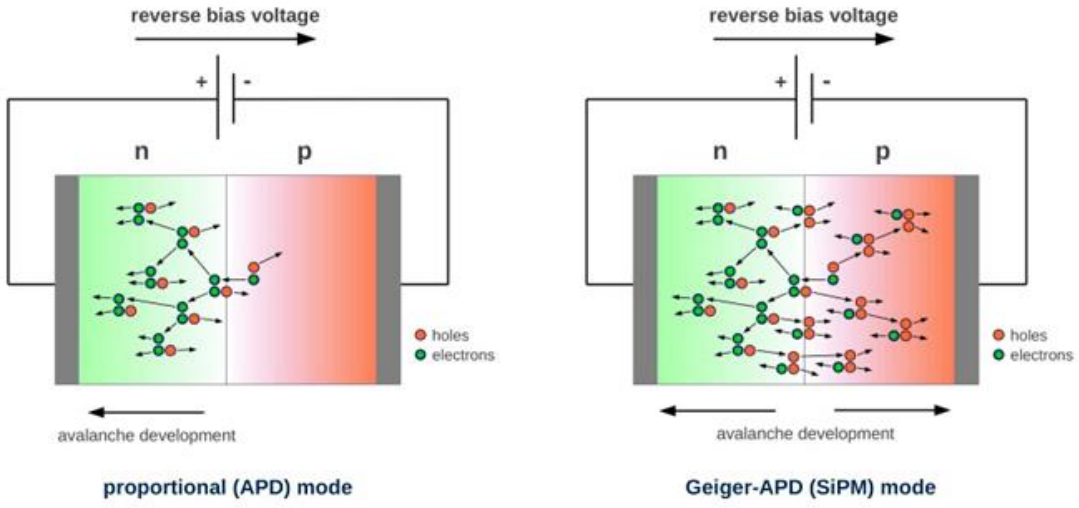

Fig.6 - Difference between proportional APD and Geiger mode APD (SiPM).
Image from Stefan Gundacker “Pratctical use to using SiPM” CERN presentation 7th of June 2015

However, the limit of a single G-APD cell is the non-linear response, because the output signal is fixed, regardless the number of photons which hit its active surface.

1.6.1 Noise sources in G-APD sensors

1.6.1.1 Dark Count rate

As consequence of high value of electric field inside this kind of detector, thermally generated electron-hole pairs also can induce avalanches and it is not possible to distinguish the electrical current produced by the arrival of a photon from that derived from electron-hole pairs created by thermal fluctuations in silicon. As consequence, dark current increases with thermal state and may double approximately every 10°C of temperature increase. As consequence, breakdown voltage decreases as the temperature increases.

Furthermore, since the probability of generating an avalanche depends on the bias voltage, if the applied polarization is increased much, the rate of dark counts increases accordingly (Fig.7, Dark count rate -over voltage dependence).

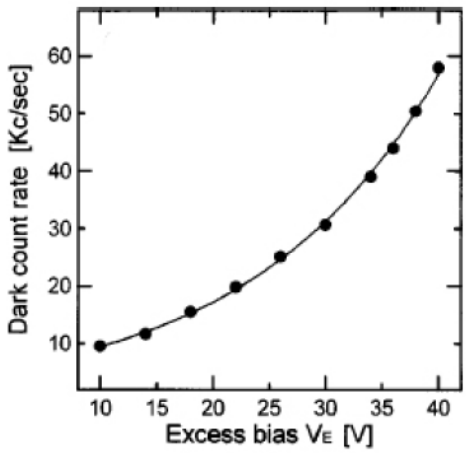

Fig.7 -Dark count rate as function of applied overvoltage.

Due to the thermal contribute, dark current increases with thermal state and may double approximately every 10°C of temperature increase.

1.6.1.2 After-pulses

Another factor that contributes to worsen the signal-to-noise ratio in the G-APDs are secondary discharges, named *after-pulses*, which can occur subsequently to the primary ones provoked by photon absorption or thermal fluctuation.

When an avalanche develops, it may happen that some carriers are caught by impurities of crystal lattice semiconductor and then released later, producing a new discharge, which generates output pulse. In the event that the secondary avalanche is triggered before the G-APD return to static condition (i.e. a photoconductive cell ready to accept photons), an after-pulse is distinguishable from a true signal. Instead, if the secondary discharge is triggered after the restoration of system static condition, the consequent signal will be equivalent, and thus not distinguishable, from a true photonic pulse, increasing in this manner the basal detector noise.

1.7 Silicon Photomultipliers (SiPM)

In the last years, a new class of solid state detectors, the Silicon Photomultipliers (SiPMs), are ever more becoming an alternative of the conventional photomultipliers (PMTs), thanks to their useful properties, such as: low operating voltage (25-70 Volt), solid-state and rugged constitution, miniaturized size, high quantum efficiency, fast response time (ns), good Photon Detection Efficiency (PDE), magnetic field insensitivity (Bondarenko et al., 2000) (Buzhan et al., 2003).

Conceptually, a Silicon Photomultiplier (SiPM) is a matrix of pixel semiconductor photodiode, where the pixels are joint together on common silicon substrate. Each SiPM pixel operates in limited Geiger mode, under bias voltage of 10-20% more than breakdown voltage, so each carrier generated by photons or thermally gives rise to a Geiger-type discharge. Geiger discharges are stopped when the voltage goes down below breakdown value due to external quenching resistor Rq, mounted in series on each pixel (typical Rq value is about 100 kΩ -1 MΩ) (Dolgoshein et al., 2006).

Since Rq is significantly larger than the coupled resistance of the diode (typically a few hundreds of ohm, depending on the structure of the diode), a voltage drop is developed on the quenching resistor which reduces the voltage on the photodiode to break down value (V_{bd}). If the current flowing in the is small enough that none of the carriers have impact ionization in the high field region of the pixel, the avalanche is self-quenched. Without the avalanche current, the voltage drop on the quenching resistor decreases, and the G-APD cell goes back to the idle state for the next photon detection. This resistor also serves as a decoupling element between the individual pixels. Each SiPM pixel operates as an independent photon Geiger micro-counter (like a single photon avalanche diode SPAD).

Since the SiPM pixels cooperate in parallel on a common load (Fig. 8), the output signal is a sum of the signals from all pixels hit by incident photons. Thus, a matrix of pixels,

where each element operates digitally as a binary device, works as an analogue detector, able to execute photometric tasks, as light intensity measures.

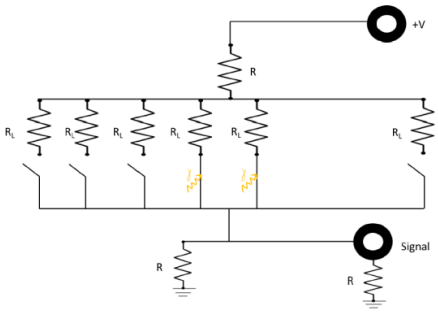

Fig.8 - The equivalent electric circuit of a SiPM: cells (G-APD pixel) are connected in parallel, and act as interrupters normally open, which close contacts when hit by photons; the resistors, in series at pixels, quench avalanches.

1.7.1 SiPM Semiconductors structure

The SiPM layer scheme is shown in Fig. 9 left: a few microns epitaxial layer on low resistive *p* substrate forms the drift region with low built-in electric field. In the thin depletion region (0.7-0.8 μm), between *p*+ and *n*+ layers, a very high electric field (3 - $5 \cdot 10^5$ V/cm) is created, producing conditions for Geiger mode discharge events (i.e. $V_{bias} > V_{breakdown}$) (Fig. 9 right). The electrical decoupling between the adjacent pixels is provided by polysilicon resistive strip and uniformity of electric field within a pixel by the n− guard rings around each pixel. All pixels are connected by common aluminum strips, in order to readout the SiPM signal (Fig. 9 centre).

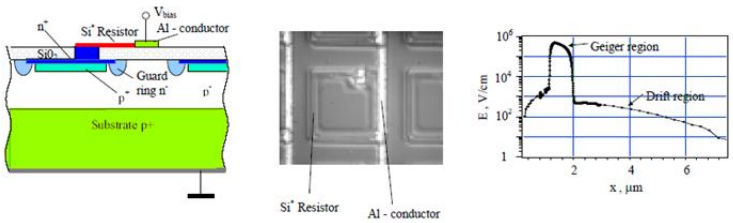

Fig.9 - From left to right: semiconductors' layer scheme; SiPM photomultiplier microphotograph; electric field distribution in epitaxial layer.

From B. Dolgoshein et al. ICFA Instrumentation Bulletin – Fall 2001 Issue https://www.slac.stanford.edu/pubs/icfa/fall01/paper3/paper3.pdf

1.7.2 SiPM Gain

The gain of an SiPM sensor is defined as the amount of charge created for each detected photon and is a function of overvoltage and microcell size. Each cell in the SiPM matrix generates a highly uniform and quantized amount of charge every time an avalanche starts. The gain of a microcell (and hence of entire sensor) is then defined as the ratio of the charge of an activated microcell and the charge on an electron. The gain can be calculated (eq. n.3) from the overvoltage ΔV ($V_{bias} - V_{breakdown}$), the cell capacitance C_{pixel} , and the electron charge, q:

$$G = C_{pixel} \cdot \Delta V / q \qquad \text{(Eq. 3)}$$

Ordinary, $C_{pixel} \simeq 100$ fF, $\Delta V \simeq$ a few Volts, so single pixel gain is about 10^6 (the same order of magnitude of correspondent vacuum PMT gain figure).

1.7.3 SiPM Photon Detection Efficiency (PDE)

The Photon Detection Efficiency (PDE) of SiPM is the probability for a photon that impact on the detector to produce an avalanche and, as in the case of single G-APD, it depends (eq. n.4) on quantum efficiency (QE), geometrical efficiency (ε_G) and on probability of generate a Geiger avalanche ($P_{trigger}$):

$$PDE\ (\lambda, V) = QE(\lambda) \cdot \varepsilon_G \cdot P_{trigger}(V) \qquad \text{(Eq. 4)}$$

The quantum efficiency (QE) of SiPM is related to the intrinsic silicon quantum efficiency, typically ≈ 80 - 90%, at working wavelenght. The geometrical efficiency ε_G, or “fill factor”, is related to the effective percentage of sensitive area of pixels. In order to ensure G-APD cells independence, between pixels are inserted insulating materials (Fig. 10). However, if a photon hits these inactive zones of SiPM, it will not be revealed.

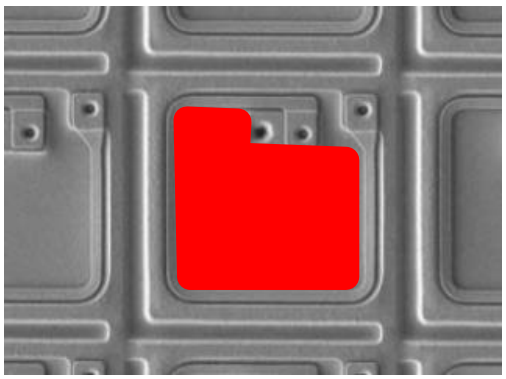

Fig.10: - a SiPM (Hamamatsu MPPC) pixel cell seen at high magnification; in red is highlighted the effective sensitive zone (fill factor).

The probability to generate a Geiger avalanche depends on the layer of semiconductor (n+ or p) where is produced the first pair electron-hole. Indeed, electrons have about a probability to generate an avalanche in the silicon double respect to holes. Therefore, if the pair is generated in the “n+” layer, the electron is adsorbed in the n+ zone and the avalanche is produced by holes. When, conversely, the pair is generated in the “p” only layer and only electrons contribute to avalanches production. The PDE depends on temperature also.

1.7.4 SiPM Dynamic Range and Linearity

The dynamic range of a SiPM sensor can be defined as the optical signal range over which the sensor provides an useful output and is a function of the total number of microcells, the overvoltage used, and the wavelength of the incident photons. Since all SiPM pixels work together on common load, the output signal is a sum of the signals from all pixels fired, the SiPM dynamic range is limited by finite total pixel number, Nm, of G-APD matrix, trough the relationship:

$$N_{ph} \cdot PDE / N_{mc} < 1 \qquad \text{(Eq. 5)}$$

where N_{ph} is the number of photons which hit the sensitive area of detector. As consequence, the number of available cells determines the probability that a pixel is interested by photonic flux. Considering that, when a pixel is fired by a photon is not temporary available for other revelation, this kind of device can exhibit a linear response until the ratio photon number/pixel is <1, otherwise the SiPM will operate in a saturation (non linear) regime. In graph reported in Fig.11 it is showed the sensor linear response at lower photon fluxes, whereas, as the number of incident photons increases, the sensor output becomes non-linear. This deviation from linearity is linked to the total number of cells in the sensor: more microcells result in a larger dynamic range. Therefore, for a given sensor size, smaller microcells will produce a larger dynamic range than larger cells.

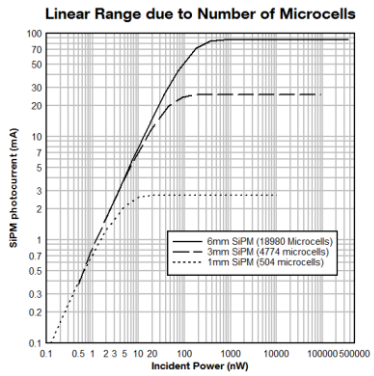

Fig.11 - photocurrent/incident power (photon intensity) response curves for different SiPM; it is noticeable that the linear range and the saturation zone vary depending on microcells (pixels) number of matrix sensor. Image from "*A Brief Introduction to Silicon Photomultiplier (SiPM) Sensors*"; paper on-line edited by ON Semiconductor,https://www.onsemi.com/pub/Collateral/AND9795-D.PDF

1.7.5 SiPM Signal shape and time response

The output signal of a SiPM cell has a pulse shape (Fig. 12) initially characterized by a "rise time", determined by the time necessary for avalanche formation and the transit times of signals arriving from sensor's diverse zones, followed by a "recovery time" of the sensor, or pulse decay time, related to cell recharge time constant, which is given by:

$$\tau_{RC} = C_{pixel} (R_q + R_s \cdot N) \qquad \text{(Eq.6)}$$

where C_{pixel} is the capacitance of a single cell, R_q the value of the cell quench resistor, N is the total number of cells in the sensor and Rs is any other resistance in series with the sensor.

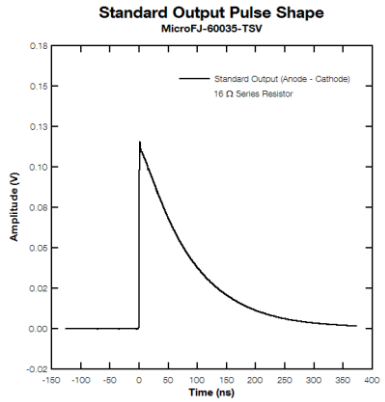

Fig.12 - Typical shape of pulse signal generated by a SiPM cell fired. Image from "*A Brief Introduction to Silicon Photomultiplier (SiPM) Sensors*"; paper on-line edited by "ON Semiconductor",https://www.onsemi.com/pub/Collateral/AND9795-D.PDF

The recovery time of the sensor (i.e. the entire cycle Geiger discharge - quenching - return to idle state) is determined by the microcell recharge time constant. This is dependent upon the various capacitances and resistances in the sensor system. Since the capacitance of the microcell will depend upon its area, the reset time will vary for different microcell sizes. Tipically, the whole "rise and recovery" sensor reactivity takes a few tens of nanoseconds.

1.7.6 Noise sources in SiPM sensor

Being essentially aggregates of G-APD cells, SiPMs share with them the same noise sources, *Dark Count Rate* (DCR) and *After-pulse*.

However, due to the specific arrangement in matrix of single cells, there is another cause of interference, the so-called *Optical Crosstalk.*

1.7.6.1 Dark Count Rate – Dark Current

The main source of noise in an SiPM is the dark count rate (DCR), which is primarily due to thermal electrons generated in the active volume. The DCR is a function of active area, overvoltage and temperature. Each dark count is a result of a thermally generated electron that initiates an avalanche in the high field region. Therefore, thermally generated electrons form a source of noise at the single photon level. If a threshold can be set above the single photon level, then false triggers from the noise can be significantly reduced. The signals resulting from the breakdown of the microcell, derived from either photon-generated or thermally-generated electrons, are identical, therefore dark counts will contribute to the measured signal, interfering with analytical contributes revelation.

Temperature modifications affects the breakdown voltage and the dark count rate of SiPMs. The breakdown voltage changes linearly as a function of temperature. However, depending on the specific SiPM technology, if large temperature fluctuations are experienced and not compensated for, it will result in changes in the effective overvoltage, which in turn affects many of the SiPMs performance characteristics. For stable operation, in the presence of significant temperature fluctuations, either bias compensation or thermal regulation are necessary. Bias compensation is the simpler of the two methods. The bias is automatically adjusted in response to a change in the temperature to ensure a constant overvoltage is maintained. If a constant overvoltage is maintained, most parameters, such as gain, PDE and timing, will remain the same as at room temperature. However, regardless of constant overvoltage, the DCR will be altered by a change in temperature, due to a change in rate generation of thermal electrons in the sensitive volume. Similarly to G-APDs, for every 10 °C of reduction in device temperature, there is about a 50% decrease in the dark count rate (and the converse is also true).

Since the dark count is comprised of a series of pulses, its magnitude is quoted as a pulse rate (kHz), or pulse rate per unit area (kHz/mm^2). This value is critical for SiPM based

instruments functionality, especially at room temperature, therefore sensors' producers have tried to minimize, in particular, this noise's figure in subsequent SiPM generations.

For continuous and integrated measurements, it is sometimes more convenient to consider this contribution as a "Dark current". As consequence of proportionality between Dark Count and sensitive surface, sensor's area is generally limited to tens of square millimeters for single device.

1.7.6.2 Optical Crosstalk

Optical crosstalk is a function of overvoltage and is also affected by the fill factor of a sensor. During avalanche, accelerated carriers in the high field region will emit photons that can initiate a secondary avalanche in a neighboring microcell. These secondary photons tend to be in the near infrared (NIR) region and can travel substantial distances through the silicon. The crosstalk is the defined as the probability that an avalanching microcell will cause an avalanche in a second microcell. In this case the sensor, which, in the absence of crosstalk should produce a signal corresponding to a single fired cell, actually outputs a signal corresponding to two cells turned on.

Crosstalk pulses, of course, can be generated starting from a dark count, or following avalanches create by absorption of photons. Thus, if many photons hit the SiPM surface, many pixels light up at the same time and each of these can either originate a crosstalk. In order to reduce optical crosstalk, physical trenches are been introduced, to separate neighboring pixels and avoid direct optical communications between them.

.

1.8 SiPM applications

Due to the above mentioned characteristics, such as extreme sensitivity, intrinsic fast time response, SiPM sensors are especially useful in studies of phenomena evolving rapidly over time (e.g. luminescence decay kinetics) . These systems recently are gaining ever more interest in diverse research fields, where are needed extremely high sensitivity for radiation, such as experimental particle physics (J.H. Kim et al. 2018), astrophysics observations (e.g. in Cherenkov cameras), (INAF web pub. 2019), critical medical applications (e.g. X-ray computed tomography used in the diagnostic imaging) (T. Maruhashi et al., 2019).

However, until now only few applications (S. Lomazzi et al, 2019) are known in applied analytical methods based on low light detection, such as bioluminescent phenomena, mainly due to the lack of practical and reliable equipment necessary to employ this class of sensor in bio-analytical laboratories or in on-field activities (LI H. et al., 2012).

1.9 Biosensors based on cholinesterase enzymes

Cholinesterases (ChEs) are enzymes present in vertebrates and insects, which hydrolyze the neurotransmitter acetylcholine (Ach) in the nervous system. In the body, ChE is responsible for nerve impulses transmission to the cholinergic synapses. The impairment of central cholinergic transmission has been related to several diseases, including Alzheimer's disease, Parkinson's disease, and schizophrenia. Acetylcholinesterase (AChE) and butyrylcholinesterase (BChE) are the two types of cholinesterase enzymes that have been widely used for the development of enzyme based biosensors.

ChEs are inhibited by several compounds including organophosphate and carbamate pesticides, nerve agents, natural toxins, heavy metals and some drugs (Songa et al., 2016).

Several cholinesterase biosensors have been developed to detect pesticides in water, food and other environmental matrices (Pundir et al.,2012; Andreescu et al., 2006).

The toxicity of organophosphate pesticides, nerve gases and of some drugs is based on the irreversible or reversible inhibition of AChE, resulting in the accumulation of acetylcholine (Ach) neurotransmitter, which interferes with muscular responses and causes respiratory and myocardial impairment and even death.

Due to high acute and chronic toxicity of these compounds, the organophosphate pesticides residue limits in food, drinking water and environmental samples are subject of regulation and control and therefore their rapid detection and reliable quantification has become increasingly necessary. Methods like gas-chromatography (GC), mass spectrometry (MS), high-performance liquid chromatography (HPLC), capillary electrophoresis (CE) and others have been developed for analysis of these compounds in contaminated samples. However, these methods present several disadvantages including the relative long analysis time, require sample pre-treatment, expensive instrumentation, highly skilled personnel and they can only be used in specialized laboratories. For these reasons there is an expanding need for field deployable analytical methods able to provide simple, fast, sensitive, selective, low cost and reliable detection of organophosphate pesticides, nerve gases and some drugs at low concentrations (Songa et al., 2016) based on their inhibition activity toward this enzyme. These methods do not identify a given molecule or nerve agent but just the potential presence of generic “inhibitors”.

1.9.1 Acetylcholinesterase biosensors

AChE catalyzes the breakdown of acetylcholine, to acetate ion and choline, AChE is mainly found in neuromuscular junctions and cholinergic chemical synapses. AchE represents the primary target of inhibition by organophosphorus compounds, including nerve

agents and pesticides. The active site of AChE comprises a catalytic coordinated triad of three amino acids: histidine, serine, and glutamic acid. The enzyme catalysis occurs when the triad's anionic binding site attracts the positively charged quaternary ammonium group of AChE. The serine hydroxyl group attacks and cleaves the ester after its deprotonation by a neighboring histidine group in the triad. The activity of AchE can be modified or inhibited by molecules called inhibitors (Songa et al., 2016). The inhibitor is a molecule that prevents the enzyme from functioning properly and modifies the speed of an enzymatic reaction.

The inhibition can be *reversible* when the enzyme can recover its biological activity, in this case the type of inhibitor can be (Engelking et al., 2015):

- competitive inhibitor;
- non-competitive inhibitor;
- uncompetitive.

In a non-competitive inhibition, the inhibitor reversibly binds at a different site from the active site of the enzyme. The active site changes conformation but can still receive the substrate; the ESI (enzyme-substrate-inhibitor) complex is formed. The turnover number goes down and the maximum speed of the enzymatic reaction decreases, while the Km remains unchanged. Instead, the uncompetitive inhibitor binds to the already formed enzyme-substrate complex and this significantly reduces the possibility for the enzyme to get rid of the product: it decreases the affinity for the substrate and the maximum speed of the enzymatic reaction.

On the other hand, in a competitive inhibition, the inhibitor has a shape similar to that of the substrate and reversibly binds to the active site of the enzyme. The competition for the active site of the enzyme depends on the concentration of the two contenders.

The affinity for the substrate (K_m) tends to apparently increase when increasing concentrations of inhibitor are present. The maximum speed of the enzymatic reaction does not change while the number of turnovers can rapidly drop to zero (Bhagavan et al., 2011).

When the inhibition is *irreversible*, the enzyme loses its biological activity because the inhibitor molecule binds with a covalent bond to a residue of an amino acid present in the active site, irreversibly modifying the shape of the active site and the conformation of the enzymatic molecule. For example, in the presence of inhibitors such as organophosphorus pesticides or nerve gases, the nucleophilic serine hydroxyl group located at the active site is covalently bound to the phosphorus atom of the organophosphorus pesticide.

Phosphorus compounds, used as nerve gases, contend the active site of acetylcholinesterase with acetylcholine. Acetylcholine is not cleaved in its inactive products (choline and acetic acid) and urges muscles to contract repeatedly causing convulsions and even death.

In the past years several AChE-based inhibitor biosensors have been developed, based on different detection priciples . These biosensors have emerged as simple, rapid and highly sensitive tools for pesticides analysis, drug screening and also for forensic applications (Guardigli et al, 2005, Pundir et al, 2012, Andreescu et al., 2006).

More recent AChE inhibition-based biosensors are based on potentiometric and amperometric transduction mode (Wang. et al, 2003; Schöning et al, 2003).

Generally, the amperometric inhibition biosensors are more sensitive than the potentiometric biosensors. The potentiometric AChE biosensors detect Ops in a single step, using a range of pH-sensitive transducers, varying from the traditional pH glass electrodes to the ion selective field effect transistors. The equipment is simple and involves the use of commercially available devices (Wang et al., 2003).

Chemiluminescent assays based on coupled enzymatic reactions have been also developed for AchE detection and for the evaluation of AchE inhibitors (Guardigli et al, 2005; Pasini et al., 1998). These assays are very rapid and can be applied for the screening of inhibitors drugs including butyrilcholinesterase and oxidases enzymes. In particular, exploiting the chain enzymatic reaction (Scheme 1), Guardigli et al. described the development of a chemiluminescent enzymatic biosensors for high throughput screening of new potential inhibitor drugs (Guardigli et al, 2005). In the following diagram is represented the chain enzymatic reaction:

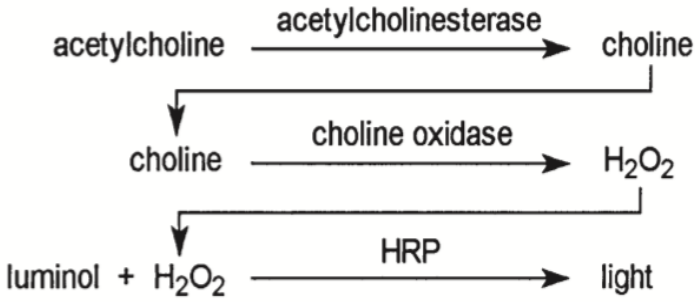

Scheme 1 Chain Enzymatic Reaction Scheme (Roda et al, 2000).

The CL detection of AchE activity was based on coupled enzymatic reactions involving choline oxidase and horseradish peroxidase (HRP) as the enzymes leading to light emission and using luminol solution to the detect the formation of H_2O_2 (Pasini et al., 1998; Roda et al., 2000). The activity of inhibitors of AchE has been measured by means of the CL luminol/H_2O_2/HRP system in which, in the presence of inhibitors such as tacrine, Ach competes for the occupation of the enzyme active site, resulting in a lower production of H_2O_2 and consequently a decreased CL signal.

When acetylcholine is present, the enzymatic reaction proceeds in the right direction, leading to the formation of hydrogen peroxide by choline oxidase and therefore, leading to the emission of light, thanks to the catalysis of HRP. On the contrary, when a competitive

inhibitor, such as tacrine, is present, it competes with acetylcholine for occupation of the enzyme active site. As a consequence, a reduction in the production of hydrogen peroxide will be observed.

1.9.2 Paper-based biosensors

Paper-based Analytical Devices (PADs) represent a new alternative technology for fabricating simple, low-cost, portable and disposable analytical devices for many application areas including clinical diagnosis, food quality control and environmental monitoring (López-Marzo et al., 2016).

Paper is abundant, available in a wide range of thick nesses, lightweight and has “green” properties such as biodegradability and environmental friendless (Hu et al., 2014; Martinez et al, 2010; Bruzewicz et al., 2008, Wang et al.; 2014). Indeed, thanks to the hydrophilicity and porosity properties, paper provides a natural platform for fabricating microfluidic channels that can be operated without an external power source (Cate et al, 2015; Bruzewicz et al, 2008; Lu et al., 2009; Carrilho et al., 2009).

Paper can be easily printed, coated and impregnated with chemical/biochemical reagents representing an ideal sensing platform for developing low-cost and portable diagnostic devices (Xia et al., 2016; He et al., 2015; Eltzov et al., 2015). Currently, quantitative analytic methods used for PADs have been developed exploiting colorimetric (Tang et al., 2009; Nath et al, 2015; Wang et al., 2012), electrochemical (Sun et al., 2015; Cunningham et al., 2015), fluorescence (Velu et al., 2015), PL (Morales-Narváez et al.,2015) CL (Zangheri et al., 2015; Roda et al., 2016; Mirasoli et al., 2014; Zhou et al. 2014) ECL (Delaney et al.; 2011), and PECL detections (Sun et al., 2014). In addition, in the last years with the improvement of the detection technologies, several PADs are implemented and integrated with devices of common use such as cell phones, smartphones (Zangheri et al.,

2015), wearable technology, or other imaging devices, scanners, optical drives/disc players, and strip readers for creating new innovative devices with higher analytical performance.

1.9.3 Origami 3D Paper-based biosensors

In order to create a 3-D device, 2-D devices can be stacked together using alternating layers of patterned paper and double-sided tape. 3-D paper devices were further developed with only a single sheet of patterned paper and folded based on the origami principle.

Origami, the art and science of paper folding, is a technique in which elegant and complex 3D objects are produced from planar paper. In 2012, Ge et al. developed a sandwich-type chemiluminescence immunoassay based on 3D origami device for the detection tumor markers. This 3D origami-based immune device has the capability to separate the operational procedures into several steps including (i) folding pads above/below and (ii) addition of reagent/buffer under a specific sequence, showing excellent analytical performance for the simultaneous detection of four tumor markers. This paper-based microfluidic origami CL detection system provides a new strategy for a low-cost, sensitive, simultaneous multiplex immunoassay and point-of-care diagnostics (Ge et al., 2012).

Chapter 2

Aim of the Thesis

As previously reported the availability of analytical methods and biosensors that enable rapid on-field analysis is of great interest in any operative and emergency situation. During the routine screening inspections carried out by the police, it is difficult, and in many cases impossible to obtain an accurate identification of unknown substances. Such operational difficulties can obstacle the subsequent confirmation step necessary for judicial purposes. Moreover, analytic techniques require highly trained personnel, remaining thus restricted in the availability of specialized units (e.g. CBRN squad) or in second-line specialized forensic laboratories.

The final effect is a broad underestimation of crimes, especially in relation to smuggling of dangerous substances. In last years, words as “NPS - new psychoactive substances”, synthetic opioids or nerve agents have been becoming common in crime reports and in press news as well. Therefore, the aim of this PhD research is focused on searching new tools and portable device suitable for implementation in routine screenings as well as in inspections and on-field activities performed by Police forces.

Among the different analytical techniques, suitable for this purpose, bio-chemiluminescent systems have been selected thanks to their potential sensitivity combined with simplicity and easy miniaturization. This approach appears even more advantageous if bioluminescence is acquired by portable devices, as smartphones, which

are capable of performing, at the same time, very sensitive light detections and rapid computational tasks.

However, even if characterized by high computational capability, approaching those of PC workstations, smartphones are often closed systems and, due to the large stack of hardware (e.g. customized filtered optical sensors) and software (e.g. firmware, acquisition apps), few parameters can be modified and generally no additional features can be introduced to tune the obtained images according to specific needs.

For this reason, besides powerful and versatile smartphone's CMOS sensors, a novel improvement in the field of avalanche photodiode was considered, the Silicon Photomultiplier "SiPM". Besides having a sensitivity that competes with traditional PMT, this class of sensors can be driven with few tens of volts, employing usual discrete electronic circuits for fast signal acquisitions. Consequently, a more direct signal acquisition can be obtained, without unnecessary intermediate steps, in the perspective of developing simplified instruments, exploitable both in remotely controlled and totally standalone conditions.

To investigate the suitability of these detectors for bio/chemiluminescence biosensors, experiments have been performed with both technologies, acquiring, as initial reference, bioluminescent emissions of two luciferase systems emitting at different wavelengths. This selection was consequent to the fact that SiPM sensitivity is optimal in the blue region of the visible spectrum, with a maximum corresponding to the emission peak of the Nanoluc (λ_{max} 490 nm), while it decreases of about 5% in the green region (λ_{max} of PpyGRT 550 nm). Moreover the feasibility of integrating a chemiluminescent enzyme-based biosensor was evaluated with an acethycholinesterase paper-based sensor for nerve agents. These effect-based biosensors could be the first-level approach where the identification of the analyte is difficult and not necessary. A strong inhibition of this enzyme in a terroristic attach offers a potent tool to rapidly evaluate the potential toxicity and lethality of the event.

Chapter 3

Development of a portable SiPM-based device for bio-chemiluminescence detection

3.1 Materials and methods

In order to develop a suitable and affordable device for on-field bio/chemiluminescence detection, the ArduSIPM, commercially available from www.robot-domestici.it, was selected. It incorporate all fundamental circuits needed to steer, easily and with low-power consumptions, a SiPM sensor. For photon detection experiments, Hamamatsu SiPM, model MPPC 13360-1325CS, sensor connected to the ArduSiPM board signal inlet was employed.

3D CAD software FreeCAD ver. 0.18 was used to design a specific black-box container for the SiPM, in this work named **LuminoSiPM**, able to mount in its inner cavity two types of interchangeable and disposable sample-holders, one useful to analyze liquid reactants and samples, the other to accommodate an origami paper-based device, for in-situ experiments.

The LuminoSiPM black-box parts were then realized in PLA polymer (Polylactic acid) by a 3D filament extruder printer (3DiELLE - ver. L). In order to obtain a better quality of realization, respect to PLA parts, regarding the fine details grade required by internal mechanical coupling, and a more structural continuity (less porosity), sample holders were printed in a UV sensitive resin by a stereo lithography (SLA) 3D printer (Anycubic Photon), able to reproduce details as precise as 50 μm.

3.2 Results and discussion

ArduSiPM is an all-in-one SiPM detector developed by Dr. Bocci research group of the INFN of Rome (V. Bocci et al. 2014). Differently from typical laboratory equipment, based on huge photomultiplier tubes and discrete data acquisition electronics, ArduSiPM is based on the microcontroller of Arduino DUE, exploited as processor board, and on a "shield", piggyback custom designed board.

Arduino DUE is an open hardware development board based on high integration mixed signal electronics Atmel SAM3X8E 32 bit ARM® Cortex-M3 CPU, widespread in the makers community, with a free integrated development environment (IDE), useful to create specific software applications. Although its compactness and affordable price (few tens of €), the Arduino DUE board expresses all the feature of the SAM3X8E microcontroller: 54 digital input/output pins (of which 12 can be used as PWM outputs), 12 ADC analog inputs, 4 UARTs (hardware serial ports), a 84 MHz clock, 2 USB OTG capable connection, 2 DAC (digital to analog converters (Fig. 13-14); all of these circuits represents what is needed to support fast analog signals acquisition and conversion.

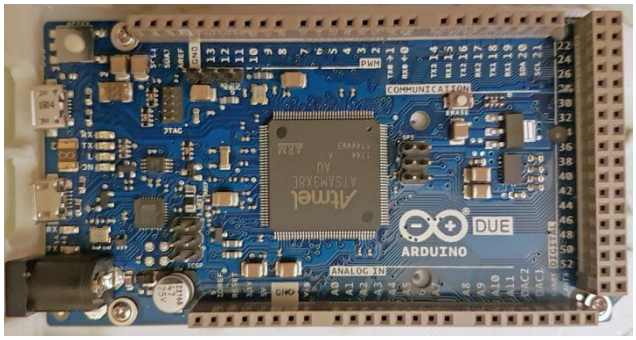

Fig.13 – An Arduino Due board - CPU/microcontroller

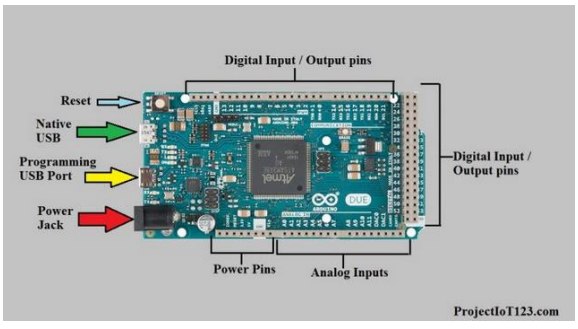

Fig.14 – Arduino Due input/output ports scheme. Image from https://projectiot123.com/2019/05/09/arduino-due-for-beginners/

The ArduSiPM Shield (Fig. 15-16), is a board which ensembles essential electronics features, using state of the art electronics for fast signals, both to monitor, to set and to acquire the SiPM signals (Fig.17).

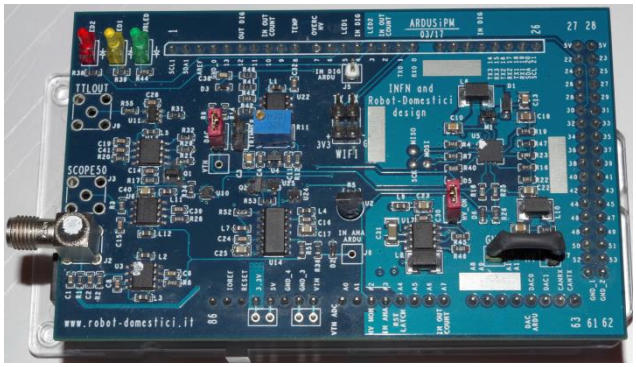

Fig.15 – The ArduSiPM shield board, view of configuration and control side.

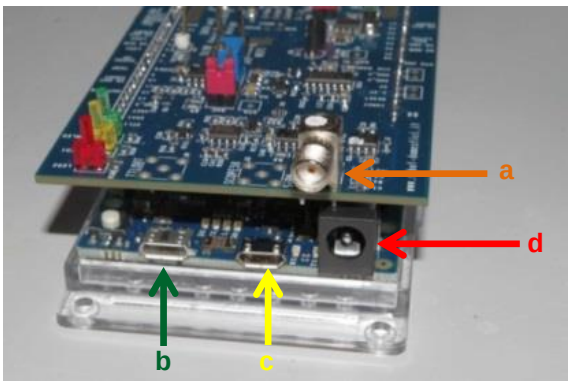

FIG.16 - ArduSiPM shield mounted on an Arduino DUE board: the SMA connector "a" is the SiPM sensor inlet port; just below, USB ports "b" and "c" and mini-jack connector "d", of Arduino platform, ensure data communication and power supply.

Using the microcontroller board, the number of photoelectron pulses can be measured in an acquisition window (typically one second), together with the number of photoelectrons (measuring the pulse height) and arrival time of each photoelectron flash. Originally, this system was developed as particle detector for high energy physics; this function is easily performed by coupling a scintillator material with the SiPM; the scintillator emits photons when it is crossed by particles with energy of the order of MeVs. Without the scintillator device, the ArduSiPM's SiPM alone can be used, in dark environment, behaving as highly sensitive photon detector.

In this research work we exploited this technology to measure bio-chemiluminescence, in order to demonstrate that the sensitivity of SiPM sensors is comparable to expensive bench-top instruments based on photomultiplier. Moreover, the small footprint, the lightness and the possibility of using it on batteries of ArduSiPM makes it really appealing for possible on-field uses.

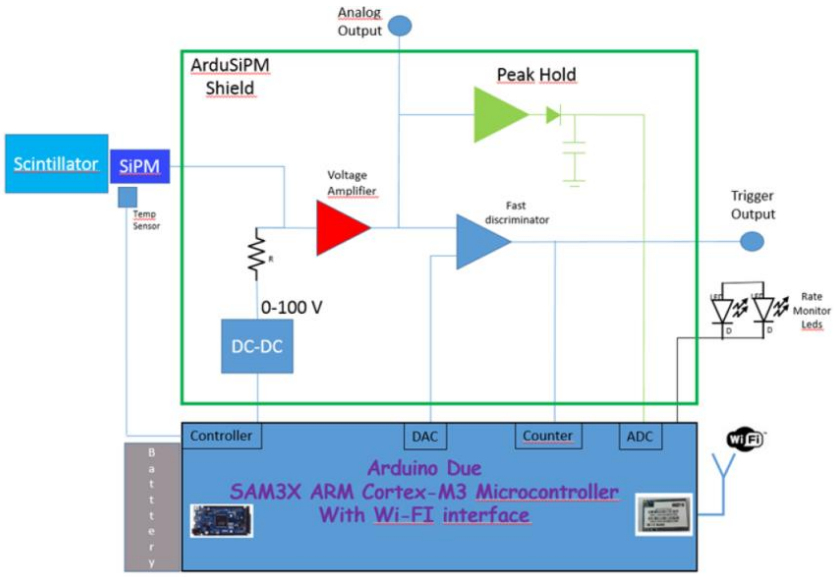

Fig.17 - Architecture of ArduSiPM: there are an external SiPM with a temperature sensor, an internal digital controlled DC-DC converter as voltage supply of the SiPM , a voltage amplifier , a fast discriminator with a programmable threshold, a peak hold circuit for pulse amplitude, leds for monitoring, all outputs from analog circuit and digital controls are connected to the Arduino DUE board

3.3 Hamamatsu MPPC SiPM sensor

The detector SiPM adopted for my research thesis is the Hamamatsu MPPC 13360-1325CS (MPPC stands for “Multi-Pixel Photon Counting”, the brand name given by Hamamatsu to its proprietary SiPM technology). MPPCs are SiPM based on G-APDs matrix, with “Reach-Through Epitaxial n+-p-π-p+“ structure; the quenching resistors are realized by deploying a layer of ≈ 0,1 – 0,2 μm of SiO_2, above the n+ layer. The detector spectral response peak is in the visible region, about at 450 nm; typical driving voltage are in the order of 50-60 V or less (Fig. 18).

Since each SiPM has its own characteristics of “operative voltage Vop” ($Vop=V_{break\ down}+5V$), the producer characterizes them individually. In this case, the sensor has been declared for an operative tension Vop=56,45 V and a leakage current “Id” (the intrinsic current which flows in the circuit, even when the sensor is not illuminated) of 0,013 μA at 25 °C.

MPPC (Multi-Pixel Photon Counter) | **S13360 series**

Selection guide

Type no.	Pixel pitch (μm)	Effective photosensitive area (mm)	Number of pixels	Package	Fill factor (%)
S13360-1325CS		1.3 × 1.3	2668	Ceramic	47
S13360-1325PE				Surface mount type	

Electrical and optical characteristics (Typ. Ta=25 °C, unless otherwise noted)

Type no.	Measure-ment conditions	Spectral response range λ (nm)	Peak sensitivity wavelength λp (nm)	Photon detection efficiency PDE*4 λ=λp (%)	Dark count*5 Typ. (kcps)	Dark count*5 Max. (kcps)	Terminal capaci-tance Ct (pF)	Gain M	Break-down voltage VBR (V)	Crosstalk probability (%)	Recom-mended operating voltage Vop (V)	Tem-perature coefficient at recom-mended operating voltage ΔTVop (mV/°C)
S13360-1325CS	Vover =5 V	270 to 900		25	70	210	60	7.0 × 10^5		1	VBR + 5	
S13360-1325PE		320 to 900										
S13360-3025CS		270 to 900			400	1200	320					
S13360-3025PE		320 to 900										

Fig. 18 - Characteristics of MPPC 13360-1325 CS SiPM sensor

This kind of SiPM is based on a 2668 G-APD pixel matrix, with a pixel pitch of 25 μm, an effective photosensitive area of 1.3x1.3 mm and a fill factor of 47% (Fig.19a-d). The declared maximum PDE of this sensor is 25% at 450 nm (Fig. 20-21).

a

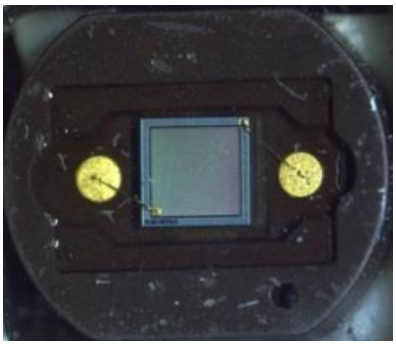

b

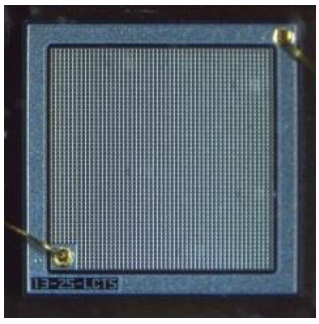

c

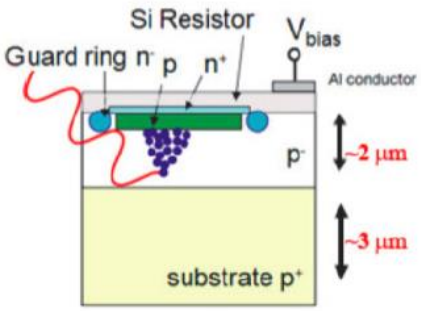

d

Fig.19 – a) Hamamatsu MPPC 13360-1325CS SiPM; b) MPPC 13360-1325CS front view; c) Close-up of sensor with the matrix of G-APD cells; d) Hamamatsu MPPC layers scheme of a single cell (A-GPD) of matrix

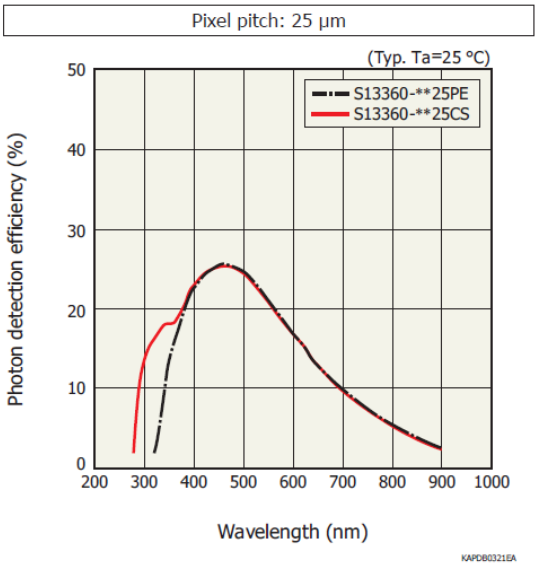

Fig. 20 -Photon detection efficiency (PDE) of Hamamatsu MPPC 13360-1325CS SiPM vs λ. The maximum is at λ =450 nm

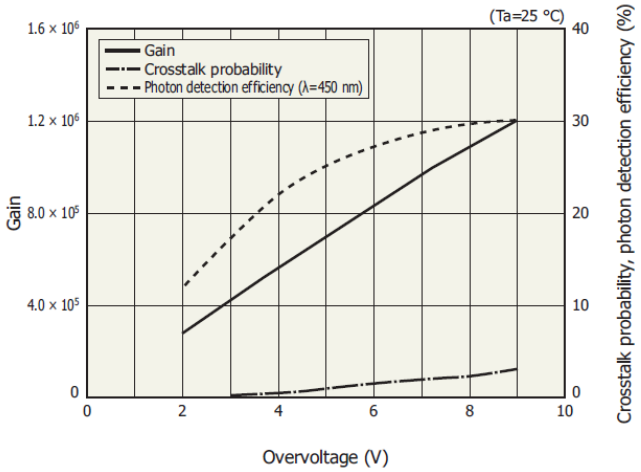

Fig. 21 - Gain, PDE and crosstalk of MPPC 13360-1325CS vs overvoltage

With the aim of employing this class of detector in simple, portable photometric instruments, it is really relevant that the manufacturer declares for them extremely low dark-currents, and significantly reduced noises figures of crosstalk and after-pulses, compared to previous products, suitable for working at ambient temperature (Fig. 22). Moreover, it is extremely significant that last generations of these detectors are close to reach the PMT typical performances, reaching single photon detection (Fig.23).

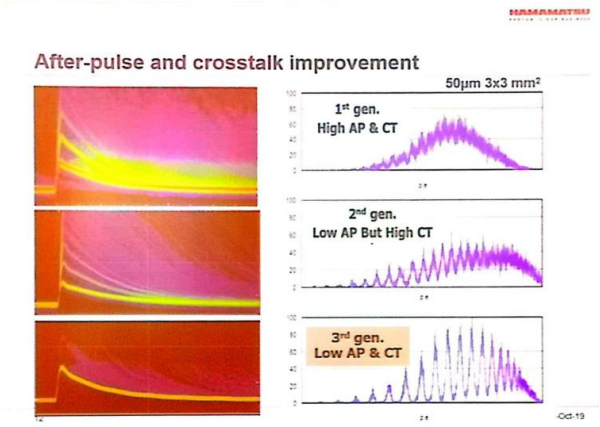

Fig.22 – Improvements, related to subsequent generation of Hamamatsu MPPC-SiPM, in After-pulse and Crosstalk noise.

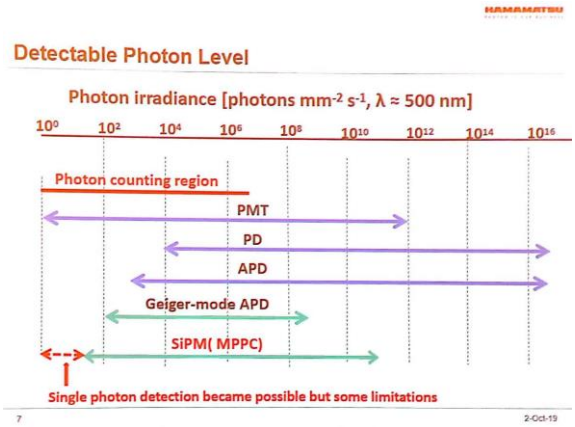

Fig. 23 – Improvements of Hamamatsu MPPC-SiPM, in reaching PMT's photon level detection performances

3.4 The LuminoSiPM analysis device

Starting from the idea to employ a SiPM sensor, not as standalone system for detecting casual events (e.g. coupled with a scintillator for cosmic ray sampling), but rather as a true luminometer, it was necessary to prepare a suitable device, in order to manage bioluminescent experiments in practical manner.

3.4.1 The black-box container

For this purpose, a two-part black-box named “LuminoSiPM”, was designed by a 3D CAD software (FreeCAD ver. 0.18) (Fig. 24-25) and realized, for a preliminary prototyping, by 3D printers. The top part of box contains an inner cavity, where the detector is housed (Fig.24); the bottom part represents the complementary closing section, inside which are placed interchangeable (disposable) sample-holders (Fig.25). Both these elements were printed in PLA polymer (Polylactic acid) by a 3D filament extruder printer (3DiELLE - ver. L).

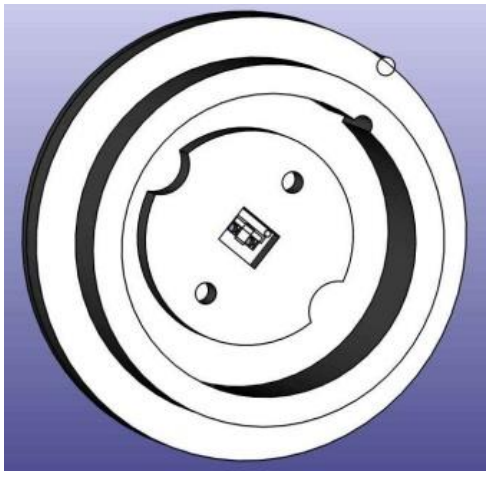

Fig.24 - Top part of LumiSiPM; in the centre, the sensor (SiPM) housing cavity.

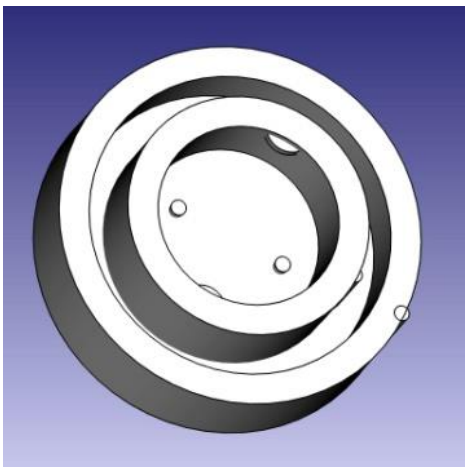

Fig.25 - Bottom part of LuminoSiPM; the bay for disposable sample-holders.

Due to its mechanical simplicity, the printed device resulted operationally versatile and easy to inspect for maintenance operation (Fig. 26-28).

Fig.26 - External side of LuminoSiPM top box; sensor contacts (56 V) are protected by an insulated cover.

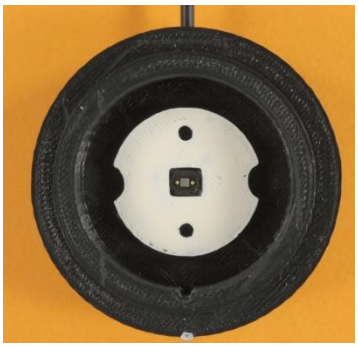

Fig.27 - Inner side of LuminoSiPM top box; the SiPM sensor is placed in the container central axial point.

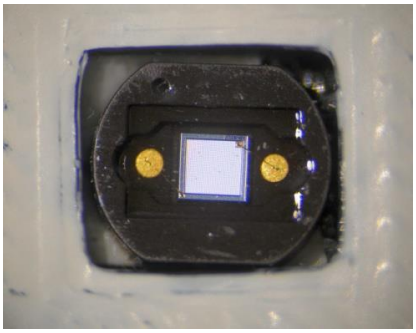

Fig. 28 - Particular of SiPM sensor housing.

3.4.2 Interchangeable (disposable) sample-holders

The inner cavity of black-box is designed to accommodate interchangeable (disposable) sample-holders, made of resin discs, shaped in two different version: the first (Fig.29), with a central cylindrical well (dimensions radius 1,75 mm, height 3 mm - inner volume about 30 μL), useful for liquid samples analysis; the second (Fig.30), with an inner, square cavity to host a foldable paper disposable device, so called “origami”, to perform in-situ bioluminescent reactions.

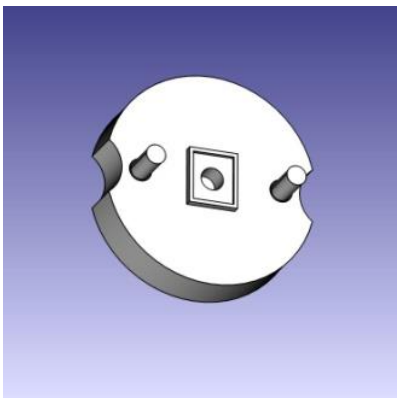

Fig.29 - Interchangeable sample-holder, version for liquid reactants.

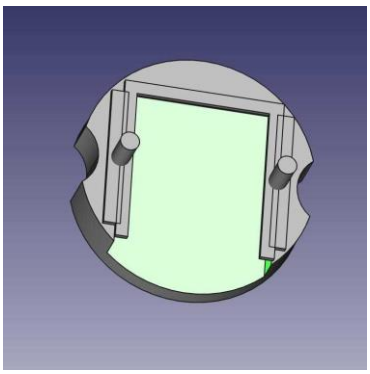

Fig. 30 - Interchangeable sample-holder, version for “Origami kit.

The interchangeable sample-holders system (Fig.31-33) is intended to manage both single and series of analyses, without automated assistance (e.g. auto-sampler). However, especially for on-field applications, it might result a valid approach, allowing to employ clean disposable accessories for each sampling and analysis.

Fig.31 - Bottom part of box, with inserted a sample-holder for liquid reactants.

Fig.32 - Bottom part of box, by its sides the two kind of sample-holder, for liquids (left), for Origami (right)

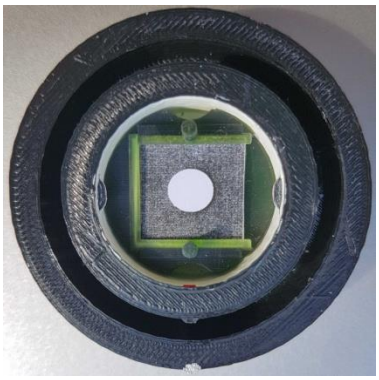

Fig.33 - Bottom part of box, with inserted a sample-holder for origami paper disposable device.

Resin discs, differently from outer box parts, were fabricated using a UV sensitive resin by a stereo lithography (SLA) 3D printer (Anycubic Photon - Fig.34). This choice was due to the necessity of having a superior quality in comparison to PLA parts, both in terms of fine details grade, required for internal mechanical coupling, and structural continuity (less surface porosity), the latter being an essential parameter to manage liquid samples.

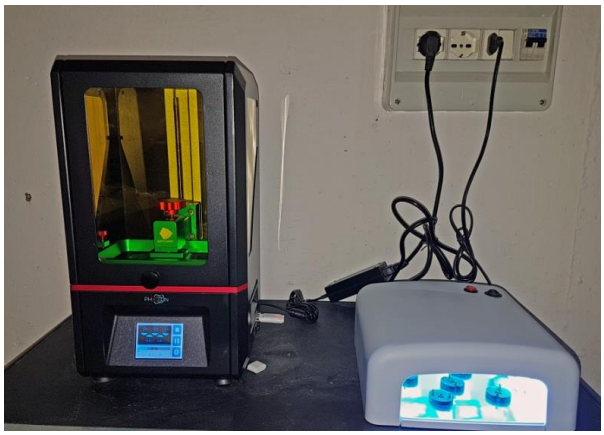

Fig. 34 – The SLA 3D printer (Anycubic Photon) employed to realize sample-holders: on the left, the printer; on the right, the UV box, for final curing stage of printed pieces.

Moreover, thanks to multiple complementarities between recesses and inserts, it can ensure the necessary darkness conditions to efficiently manage even extreme-sensitive sensor, such as SiPMs, without other light-sealing shrewdness.

Noteworthy, due to the complete polymeric composition and insulation of sensor contacts (operating at 56V), LuminoSiPM is a safe-operating device, which can be handled without necessity of electrical-shock countermeasures (Fig.35 a-d).

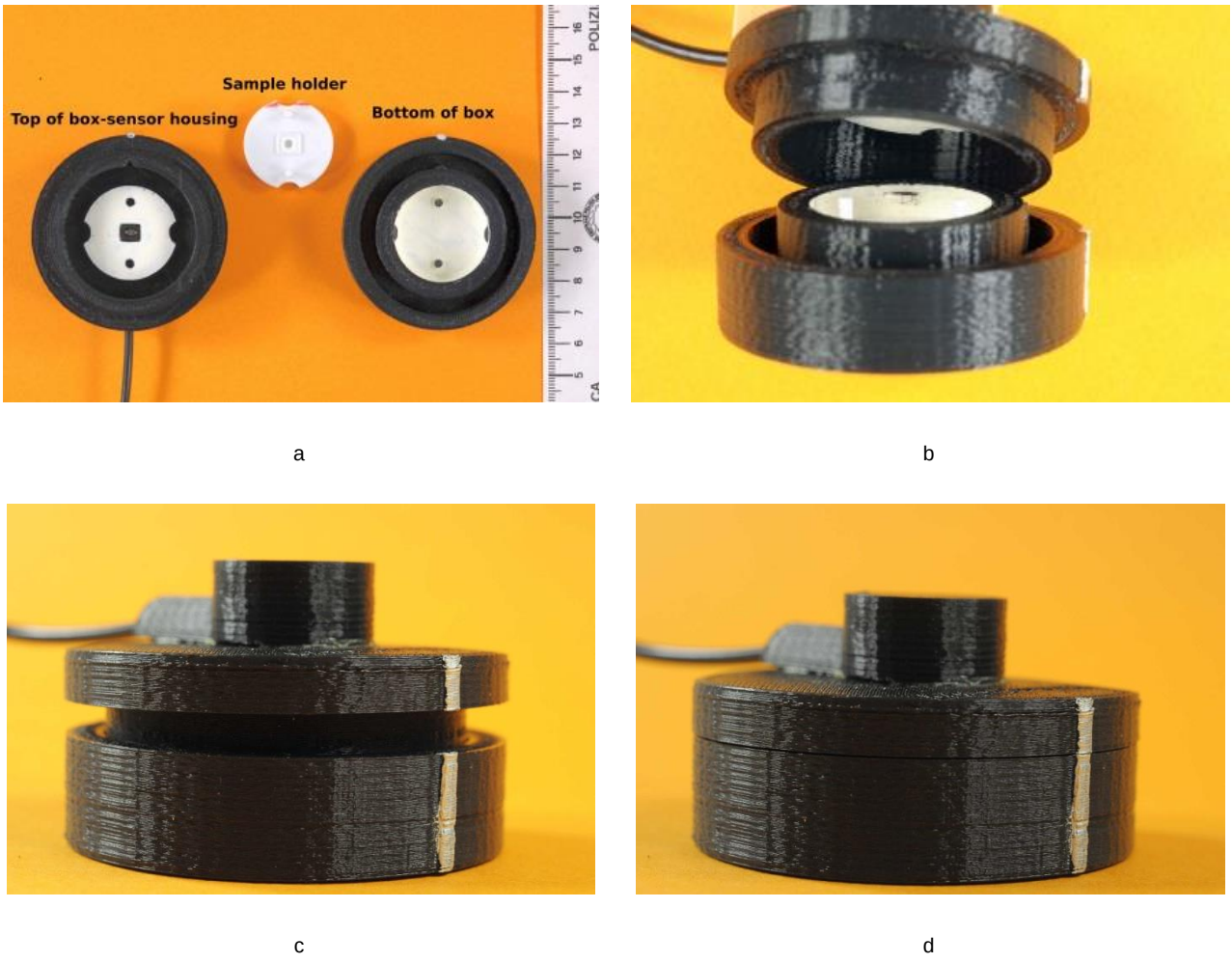

Fig.35: a) The three components of LuminoSiPM; b) The mounting of black-box, after the sample-holder has been inserted in; c) Multiple complementarities of recesses and inserts guarantee the necessary light-tightness of cell; d) The box closed and ready for measaurement.

Possible issues, related to positioning of removable sample-holders in the box, are minimized by specific point of reference and correspondent mechanical protrusions in box parts. In this manner, when LuminoSiPM box is operative, samples are always placed in the same position, directly in front of the detector, at about 1.5 mm from its sensitive surface, as is showed in 3D CAD cutting section images (Fig.36-37) of assembled cell.

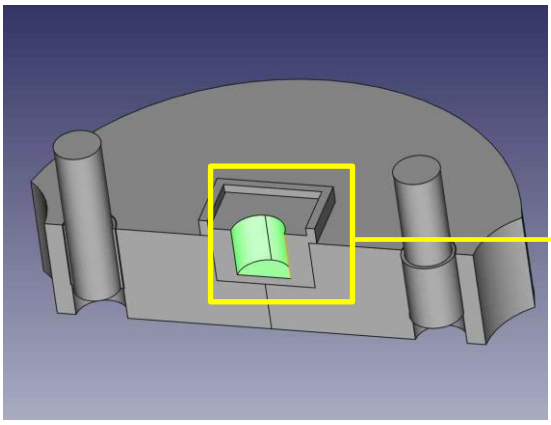

Fig.36 – 3D CAD cutting section of an interchangeable sample-holder for liquid reactants. The sample volume (green zone) is about 30 μL

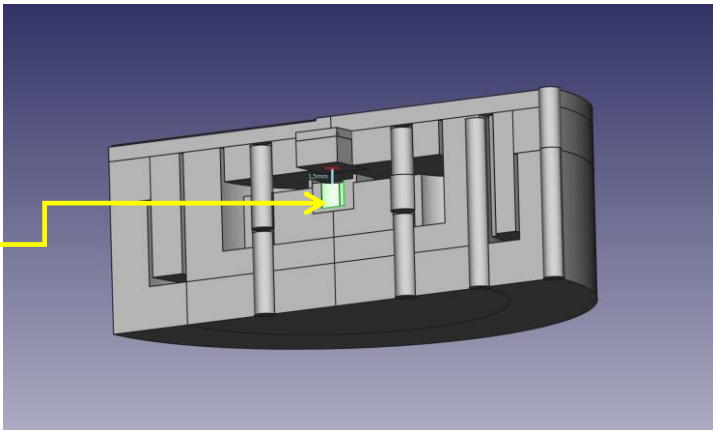

Fig.37 - 3D CAD cutting section of a mounted LuminoSiPM – the distance sensor SiPM (red point) – sample (green zone) is 1,5 mm

3.5 Experimental condition for bioluminescent signals acquisition

During measure sessions, ArduSiPM was contained in a plastic box electrically insulated and removable, for easy inspections on functionality and operative conditions (Fig.37 a-b). LuminoSIPM cell was connected to signal inlet of ArduSiPM (SMA connector); data acquired were transferred, in real-time, by an Arduino DUE USB port to a PC, for storing and software treatment.

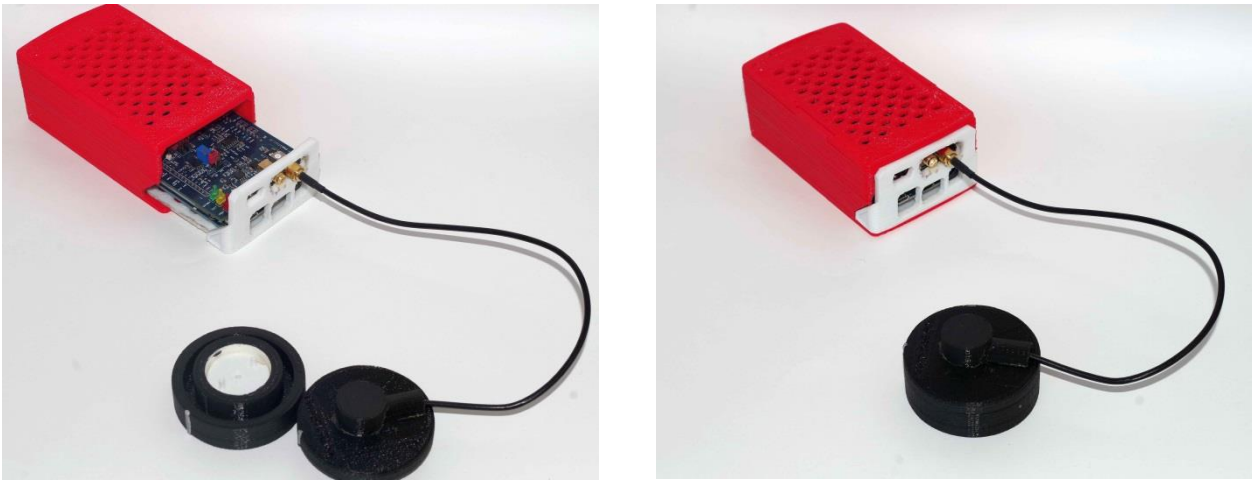

a b

Fig.37: a) ArduSiPM (red-white box,) open for inspection and connected to LuminoSiPM (black cell) ready for sample mounting; b) the instrument in measurement configuration.

Due to limited power supply requirement, all electric power was uniquely supplied by the PC USB port (5V, current max 0,5 A). However, the same result can be achieved by using USB power bank, batteries (e.g. 9V Block cell) or DC power supplies connected to Arduino inlet ports. The whole instrument (excepting the personal computer) is easily transportable in a little carrying box, useful for on-field analysis (Fig.38 a-b).

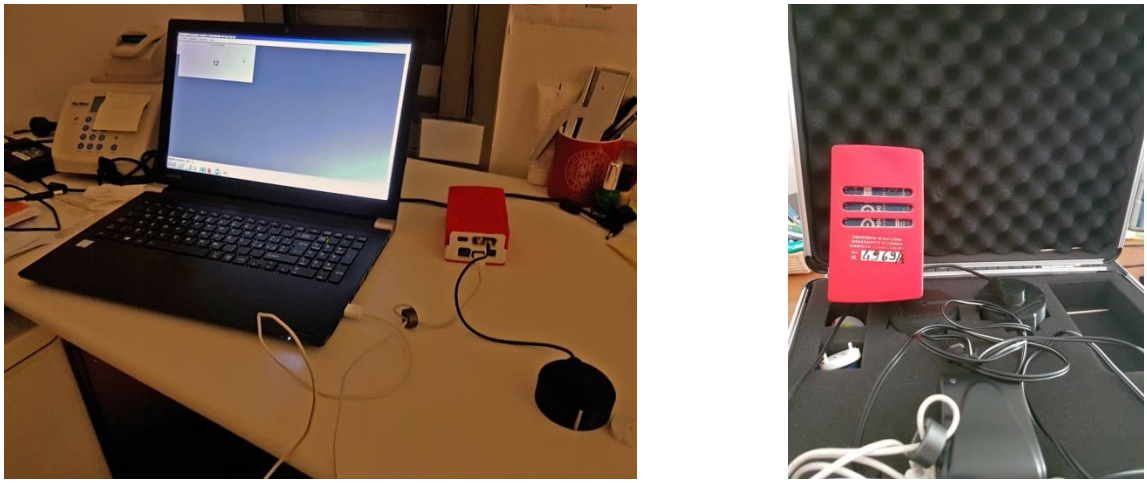

a *b*

Fig.38: a) an operative analysis session with ArduSiPM connceted to LuminoSiPM cell and to a PC for data acquisition;b) the apparatus with the box for on-field analysis.

3.6 Study of MPPC-SiPM sensor driving parameters

The practical adaptation of ArduSiPM, from particle detector to photon detection, requested care due to the different photon production process. In particle physics application, the number of photoelectron is small (>5 photons), but concentrated in few nanoseconds. In the case of luminescence, the flux is continuous and, even if the number of photons in a large time can be conspicuous, using the threshold used in particle physics (5 photoelectrons), instrument can lose all flashes with less than this quantity. This means that the threshold to be used, must be as low as possible up to the physical limit of one single photoelectron detection.

The main problem, to reach this threshold, is the dark noise. SiPMs are high sensitivity sensors, but suffer from “Dark Noise”, originated by thermal effects in lattice crystal structure of semiconductor. Therefore, the theoretical single photon response of the detector, is not actually manageable in these conditions, due to the high level of noise competition, generated by thermal excitation, which produce free electrons inside the SiPM depletion region, leading to (false) pulses and, as consequence, spurious avalanches. These happen randomly and independently from the illumination field and are not distinguishable from real photoelectron pulses. The best SiPMs in the market has a dark count, for 0.5 photoelectron threshold, of about 70-100 kHz (or counts per second) at room temperature. The 5 photoelectrons threshold (events generated by simultaneous hit of, at least, 5 photons on the same pixel of SiPM matrix) typical for physic particle researches, produce a composed dark count (the random coincidence of 5 pixel hit in few nanoseconds) near to 0 Hertz (cps).

In this research work, in order to enhance the sensitivity for extra-low signals maintaining under control the dark noise, a threshold of about 2-3 photoelectrons has adopted, to reach a manageable composed dark count rate of few hundreds of hertz (cps).

This threshold, while not reaching the physical limit of one photoelectrons, give anyway the possibility to measure very low light intensities, typical of bioluminescence and chemiluminescence reactions, with a good noise to signal ratio at room temperature with standard SiPMs.

For this reason, the ArduSiPM exploits a discriminator circuit, which allows possible to fix a voltage threshold to select a limit of admittance of signal produced by SiPM sensor. To find a right condition of signal/noise ratio, it was conducted an extensive series of acquisition of dark counts, measuring spurious signal produced by sensor in total darkness condition, without a sample charged into LuminoSiPM black box. Starting from an equivalence of 2 mV per photoelectrons (i.e. the tension produced by a photon which hit the surface of sensor), it was analysed the output signal of dark noise, expressed as count per second “cps”, varying gradually (steps of 0,1 mV) the threshold voltage of discriminator (Fig.39). In this manner, was found that, for the time of acquisition employed in bioluminescence analysis, 5 min, dark noise resulted acceptable in 3,55-3,6 mV range (equivalent to the probability that two photons hit a pixel of sensor), with figures of noise ranging between 2300 and 1900 cps at 25 °C. However, forcing the discriminator circuit towards lower voltage thresholds, the dark noise increased rapidly until several thousands of cps, making the system not useful to low-intensity photonic signals detection. Moreover, as consequence of thermal dependence, noise pulses tend to increase raising the ambient temperature.

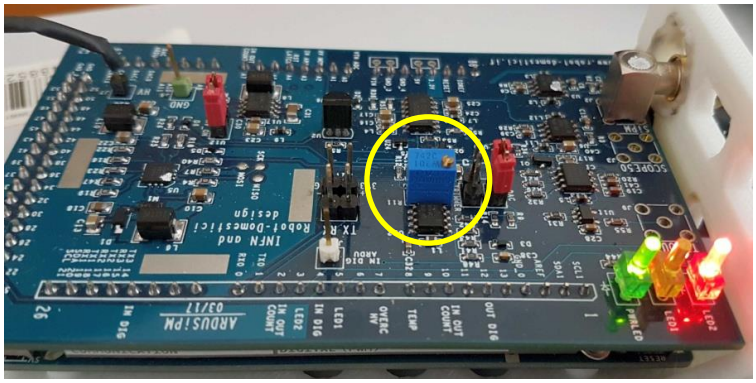

Fig.39 - an AsduSiPM in action: led lights blinking indicate the rate of photon hits recorded by sensor in selected conditions; circled in yellow, the trimmer for fine tuning of bias voltage, which manages the discriminator threshold of sensor signal.

3.6.1 SiPM signal acquisition and data treatment

The ArduSiPM platform allows to read directly detector's signal, exploiting intrinsic functionalities of Arduino board IDE (Integrated development Environment); however, for an improved treatment of luminescence signal acquisition, a specific MS Windows software for PC hardware, freely downloadable at web address https://ardusipm.filippocurti.it/download , was employed.

Sensor's signal was acquired, following bioluminescent emission kinetics, for 5 minutes, with data sampling cycles of 1 second. In this manner, a total of 300 numerical acquisitions was recorded, in form of counts per second (cps), for any single analytical experiment and stored in MS Excel format files, for subsequent interpretative treatments.

However considering that ArduSiPM output signal is transmitted in decimal format through a RS232 serial interface, at the speed of 200 KBs, as standard ASCII character flux, it is possible to acquire and treat data by any other hardware platform (e.g. Raspberry Pi3 - Pi4 class micro-boards or small microcontroller device like M5Stack), using self-customized routines, realizable with any programming language, as freely available object-oriented inter-platform environments (e.g. Python, JAVA).

These hardware and software possibilities highlight the most advantageous features of this light detection approach, connected to the possibility to control all the steps of instrument activity, starting from the sensor signal production, until the final output of data collected.

3.6.2 Preliminary dark count rate evaluation

To select the more suitable instrumental condition for analytical experiment, especially regarding the dark (thermal) noise, two series of 5 min signals acquisitions were performed, with the sensor shielded from light and varying gradually the discriminator threshold

admittance in the range 3,39 - 4,57 mV. Measures have been repeated in two different room conditions: series “A” between 24-26 °C, Series “B” between 26-28 °C.

In following graphs (Fig.40) are showed increasing trends of noise due to the variation of only 1 mV of limit threshold. Furthermore, it is noticeable that a slight increase of ambient temperature, enhances intrinsic dark noise figures of detector.

In Fig 41 are reported plots of spectra of multiple counts frequencies, related to the series “A” of dark current analysis. It is evident, examining patterns, from nr.1 (the highest Bias) to nr.8 (the lowest), that lowering the threshold polarization value produces a sudden increase both in absolute number of counts and in occurrence of state with multiple pulses (of noise). If not well considered, these last factors might affect the manageability itself of instrument, as consequence of detrimental effects on sensitivity for low intensity analytical signals.

On this experiential base, a discriminator bias voltage of 3,60 mV was selected, in order to maximize sensor sensitivity, maintaining sustainable dark noise figures (about 2000 counts for 5 minutes of acquisition).

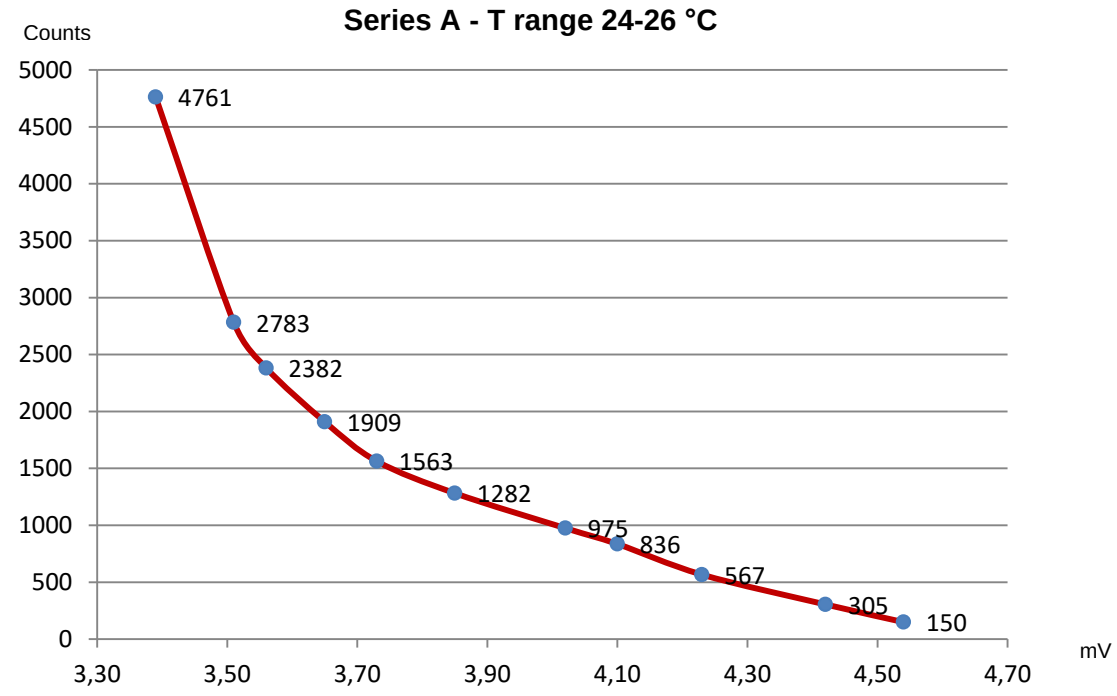

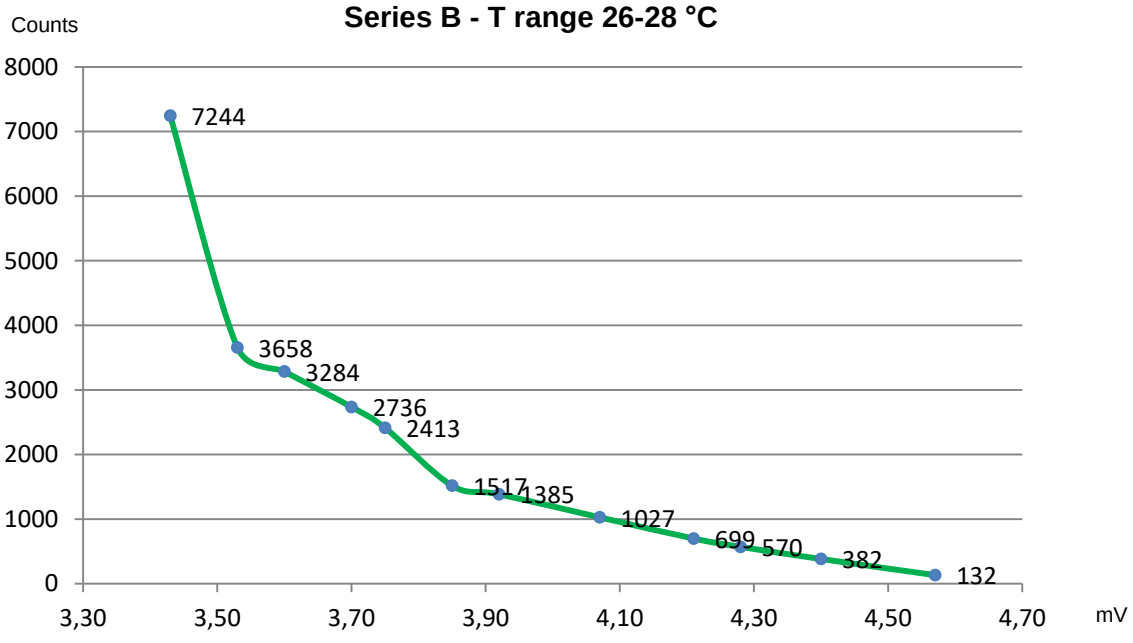

Fig. 40 - Series of SiPM Dark Noise acquisitions: Series A measures acquired at room temperature range 24-26 °C; Series B measures acquired at room temperature range 26-28 °C

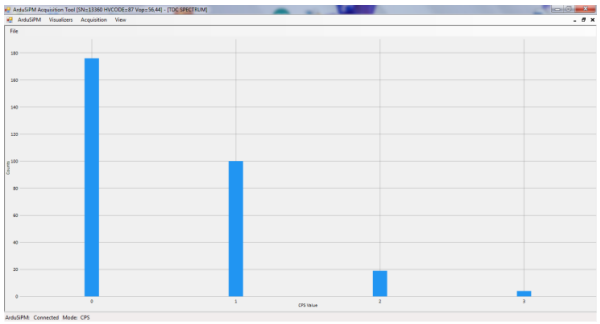

1- 4,54 mV (25,5 °C)

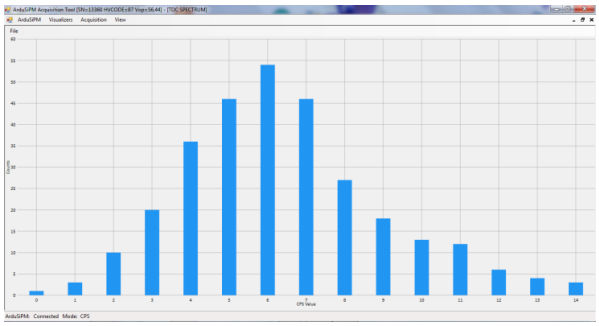

5- 3,65 mV (24,5 °C)

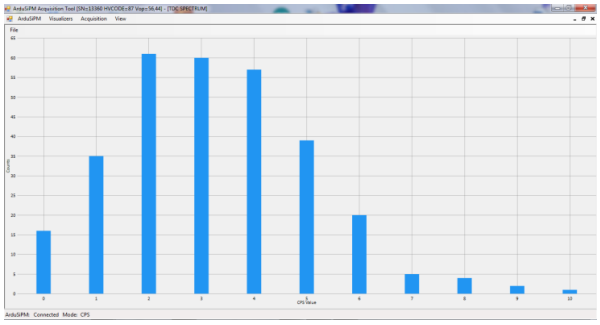

2- 4,02 mV (25 °C)

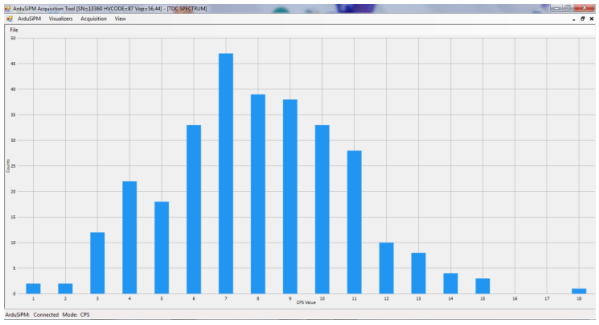

6- 3,56 mV (24,3 °C)

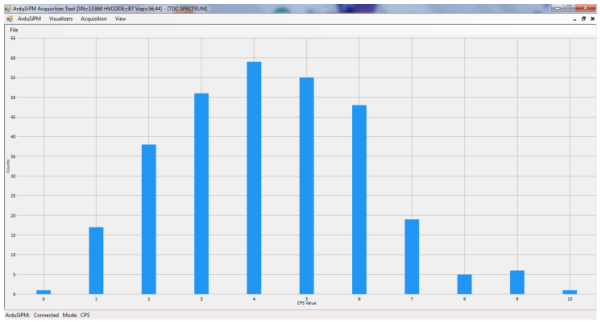

3- 3,85 mV (25,0 °C)

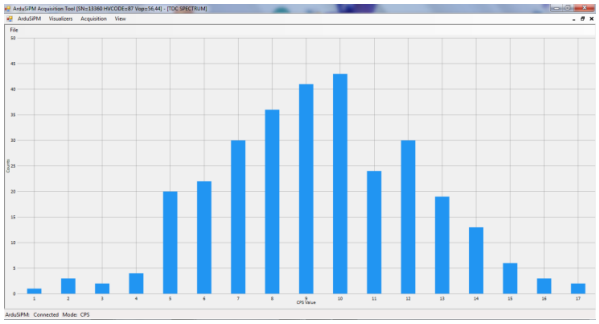

7- 3,51 mV (24,0 °C)

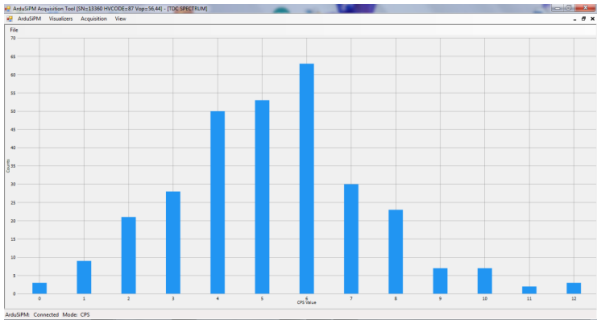

4- 3,73 mv (24,5 °C)

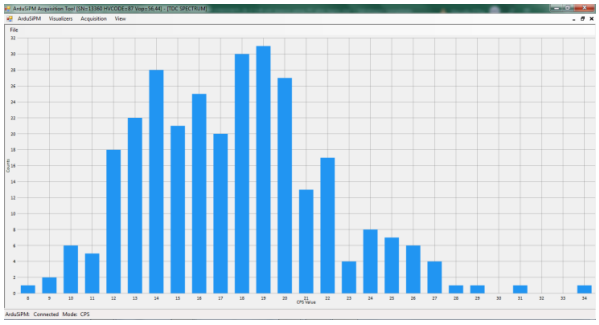

8- 3,40 mV (24,0 °C)

Fig. 41 -Frequency spectrum of dark noise generated by Hamamatsu MPPC 13360-1325CS SiPM, varying the discriminator Bias threshold of ArduSiPM driver board: in X axis are reported the cps (counts per second) values, in Y axis the correspondent frequency (number of occurrences) of each event; temperature conditions are indicated for each acquisition. Lowering the bias voltage (mV), are increasing both the absolute value of dark counts (related to plot's areas) as the probability of noisier (i.e. higher counts per second values) events.

Chapter 4

Comparison of portable light detectors performances

4.1 Materials and methods

4.1.1 Reagents and instrumentations

E. coli competent cells (JM109) for plasmid propagation and the SOC medium (tryptone 20g/L, yeast extract 5g/L, NaCl 5M 2mL/L, KCl 1M 2,5 mL/L, MgCl2 1M 10mL/L, MgSO4 1M 10mL/L, D-Glucose 1M 20mL/L) were from Sigma (St. Louis, MO, USA), while *E. coli* competent cells (BL21) for protein expression were from Agilent Technologies (Santa Clara, USA). Luria-Bertani (LB) medium and LB-Agar plates used for cell cultures were prepared with Select Agar and LB (Lennox L Broth) from Sigma (St. Louis, MO, USA) added with ampicillin (1µg/mL). All media and materials were autoclaved for 20 minutes at 121°C.

Expression plasmids, kits for plasmid extraction and purification, BrightGlo and NanoGlo substrates were from Promega (Madison, WI, USA). Enzymes required for cloning were from Fermentas (Vilnius, Lithuania). Cell lysing and protein extracting reagent B-Per was from Thermo Scientific (Rockford, USA). Protino Ni-IDA Resin and 14 ml Protino Columns required for protein extraction were purchased from MACHEREY-NAGEL GmbH & Co. KG (Düren, Germany). Microcon 30K device used for protein concentration and buffer

exchange were purchased from Merck Millipore Ltd. (Tullagreen, Carrigtwohill, Co. Cork, IRL). All other chemicals were purchased from Sigma (St. Louis, MO, USA).

Measurements were performed with Varioskan Flash multimode reader (ThermoFisher Scientific) and compared with Oneplus 6 smartphone (Oneplus, Shenzhen, China) equipped with an integrated dual camera (16 MP Sony Exmor IMX 519 sensor and F1.7 aperture + 20 MP Sony Exmor IMX 376K sensor and F1.7 aperture), and ATIK 383L cooled camera (ATIK Cameras, New Road, Norwich), equipped with a high resolution monochrome CCD sensor (Kodak KAF 8300, sensor size 17.6 x 13.52 mm) and SiPM were used as portable detectors.

4.1.2 Luciferase purification

Expression plasmids pGexNanoluc and pGexPpYPGRT for NanoLuc and PpYPGRT bioluminescent protein expression and purification were previously obtained in the laboratory.

Purified plasmids were used for transformation in BL21 competent cells (see Transformation of *E. coli* competent cell) which were plated and incubated at 37°C overnight on selective (ampicillin) LB-Agar plates. Single colonies were grown in liquid cultures (LB) and then expanded in 50mL flasks in order to obtain a large culture, necessary for protein purification (see *E. coli* cultures and purification of the recombinant proteins).

E. coli competent cells BL21 (>10^6 cfu/µg) were transformed with the purified plasmids following the standard protocol from Promega. Frozen competent cells were removed from –80°C and placed on ice for 5 minutes, in order to let them thaw. Then 70 µl of competent cells, previously added with 1 µl of plasmid DNA from each clone, was added and gently mixed by flicking the tube. Control DNA pUC19 was used as positive control, to determine the transformation efficiency. The tubes were incubated on ice for 30 minutes,

then heat-shocked for 45 seconds in a water bath at 42°C and immediately placed on ice for 2 minutes. A volume of 600 µl SOC medium preheated was added for each tube and incubated for 90 minutes at 37°C with shaking (about 225rpm). Eventually, 100 µl of cells were plated on selective agar-plates (ampicillin-added) and incubated at 37°C overnight. The same protocol was used for the purification of all bioluminescent proteins.

4.1.3 *E. coli* clone cultures and purification of the recombinant proteins

Single colonies were selected and grown in liquid cultures (LB) by incubation overnight at 37ºC, once at the appropriate optical density (OD) they were expanded in 50mL LB flasks (dilution ratio 1:10) in order to obtain a large culture; the flasks were then evenly incubated overnight at 37ºC up to the desired OD and then bacterial cells were pelleted at 4000 × *g* for 10 minutes and stored at -80ºC. For every step, the cellular light emission was checked at the Varioskan by addition of 100 µL DLH_2 1mM in citrate buffer at 5.5 pH to 100 µL of cell culture. In the meanwhile, a Cell-Lysis-Extraction buffer along with a Lysis-Equilibration-Wash-buffer (LEW Buffer) and an Elution buffer to use with purification columns were made.

Cell-lysis-extraction buffer consisted of 10µL of Lysozyme (10mg/mL) and 1µL of a serine protease, such as phenylmethylsulfonyl fluoride (PMSF) (100mM) per 1mL of B-PER Reagent; LEW Buffer was a solution 300 mM in NaCl, 50 mM in NaH_2PO_4 and adjusted to pH 8.0 with NaOH while Elution Buffer was a solution 300 mM in NaCl, 50 mM in NaH_2PO_4 and 250mM in Imidazole, adjusted to pH 8.0.

Operating on ice, the bacterial pellet was pipetted up and down until it was homogeneous by using 2 mL of cell-lysis-extraction buffer per approximately 0,5 gram of pellet and the suspension was then transferred to 50 mL centrifugation tubes, where it was incubated for 20 minutes, paying attention to gently re-suspend it every 5 minutes.

The lysate was then added with 4 mL of LEW Buffer and kept at r.t for 10 minutes, before being centrifuged at 10,000 × *g*, 4^0C for 30 minutes, to separate soluble proteins from the insoluble proteins and cellular lysate.

A 5 mL-volume of clear surnatant was then collected and subdivided in 1 mL aliquots, for a better handling, paying attention not to pipette up the fleeting pellet at the bottom of the tube.

The purification system was prepared by putting 0.5 gram of Protino Ni-IDA Resin in the respective 14 ml Protino Column. The resin was then conditioned with 8 mL of LEW Buffer and 1 mL aliquot of lysate carefully transferred to the column allowing its absorption on the resin. The column was then washed with 8 mL of LEW Buffer to eliminate unabsorbed interferents; the washing solution was collected to check the possible presence of undesired eluted target protein. The target protein elution was performed by adding to the column 1 mL of Elution Buffer at time, for 4 times, and collecting 4 different fractions, which were then analyzed at the Varioskan. All purified bioluminescent proteins were characterized using a Varioskan Flash Multimode Reader. Different buffers were tested in order to optimize protein stability and bioluminescent signal.

4.1.4 Comparison of analytical performances of LuminoSiPM with other light detectors, using different concentrations of PpyGRT and NanoLuc Luciferases.

In optimized conditions the assay procedure is very straightforward, consisting in just a few steps: a volume of 5 µL of purified protein solutions was added in the well and then acquisition is performed after the addition of 10 µL of the substrate. BrightGlo substrate was used for PpyGRT luciferase and NanoGlo substrate for NanoLuc luciferase. Different light detectors including a standard benchtop luminometer, portable CCD, SiPM and smartphone

integrated CMOSs were used to investigate the feasibility of using the purified luciferases in different settings. Varioskan Flash multimode reader was first used for evaluating the sensitivity of purified luciferases (concentration range from 1.0×10^{-1} to 1.0×10^{-6} mg/mL). BL signals were acquired for 30 min with an integration time of 200 ms. BL images of purified proteins (concentration range from 1.0×10^{-1} to 1.0×10^{-5} mg/mL) were also obtained with a cooled portable CCD camera (ATIK 383L+ mono cromo CCD) integrating BL signals for 5 min at +5°C and room temperature. Oneplus 6, was selected to detect BL signals of purified luciferases and images were taken for 30 sec with different sensitivity settings, from ISO 100 to ISO 3200. ImageJ software (National Institutes of Health, Bethesda, MD) and GraphPad Prism v.5 (GraphPad Software, La Jolla, USA) were used to analyse and to plot the data, respectively. Limit of Detection (LOD) was calculated as the blank plus three times the standard deviation. All measurements were performed in triplicate and repeated at least three times.

4.2 Results and discussion

4.2.1 Recombinant protein induction

As described in materials and methods, protein induction and purification were performed in *E. coli* BL 21 cells. The BL protein expression was induced with IPTG for 4h, at 37°C causing an increase of the BL signal equal to 3 times the non-induced. In the figure below is shown the BL kinetics of NanoLuc luciferase expressing bacteria with and without induction.

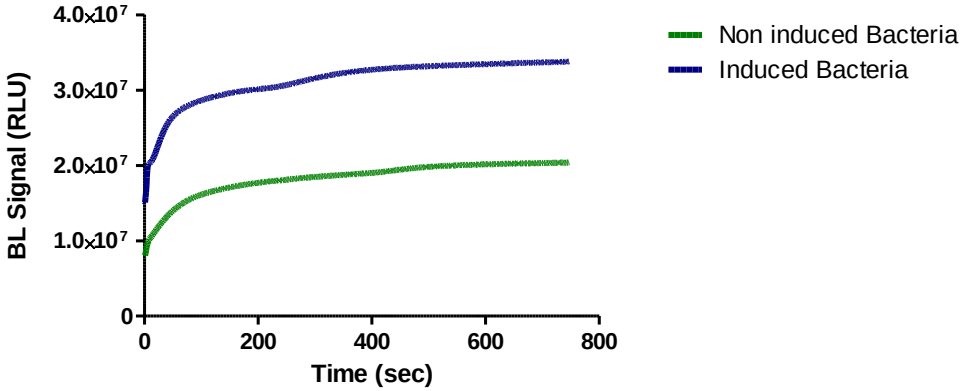

Fig.42 -Emission kinetics of NanoLuc luciferase with and without IPTG induction.

4.2.2 Protein purification

Protein purification was performed as described in materials and methods and several fractions were obtained. The bioluminescent signal and the protein concentration of each fraction was than characterized. BL signal was acquired using Varioskan Flash Luminometer and the signal obtained for each fraction is reported in the figure above (Fig. 43-44). For NanoLuc luciferase, the most concentrate fractions were F3, F4 and F5. While for PpYPGRT were F5, F6, F7 and F8. This difference in proteins retention time for the chromatographic column is related with difference in size and hydrophobicity.

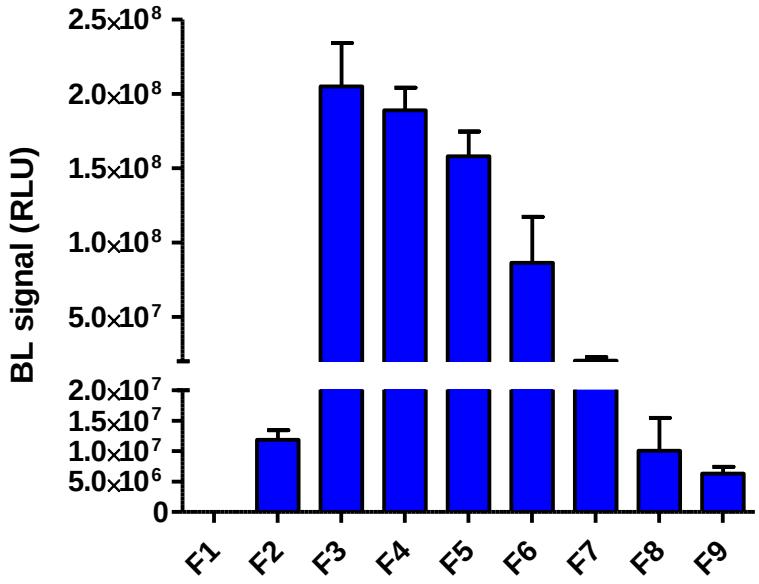

Fig. 43 - Bioluminescent signal of different purified fraction of NanoLuc luciferase

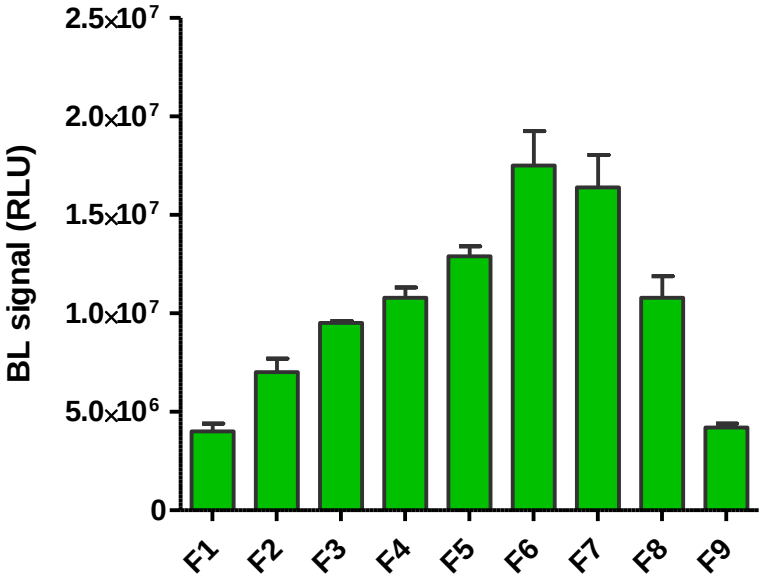

Fig. 44 - Bioluminescent signal of different purified fraction of PpYPGRT luciferase

Protein concentration was then determined with the BioRad Protein Assay system using bovine serum albumin (BSA) as the standard and purified proteins were stored at 4 °C. The total yield for purified protein was estimated to be ~2.4 mg/0.1 L culture, which is consistent with heterologous expression of luciferases in microbial systems.

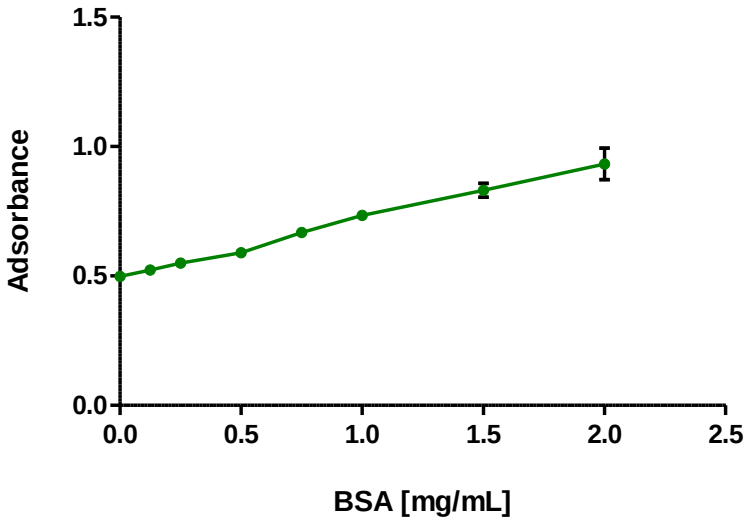

Fig. 45 - Standard calibration curve used to quantify protein concentration with the BioRad assay (R^2= 0.9923).

Protein concentration for each fraction was calculated by interpolating the calibration curve and concentrations ranging from 0.2 to 3 mg/mL were obtained.

4.2.3 Experimental conditions

The Elution Buffer used for luciferase purification (see Materials and Methods section) consisting in a 250 mM imidazole solution, is optimal for this purpose, but it has a major drawback, since it is known to strongly inhibit firefly luciferase activity. A buffer exchange is thus required and the standard approach is protein dialysis. Protein dialysis is suitable for the removal of unwanted small molecules such as salts, reducing agents, or dyes from larger macromolecules, and it is commonly used for buffer exchange and drug binding studies, however it is a long-time and multi-step process. We therefore opted for a filtering device, Microcon 30K, which allows for a fast and easy buffer exchange, as well as protein concentration, as described in section Materials and Methods. The results, in term of signal increase, are summarized in the figure n.46.

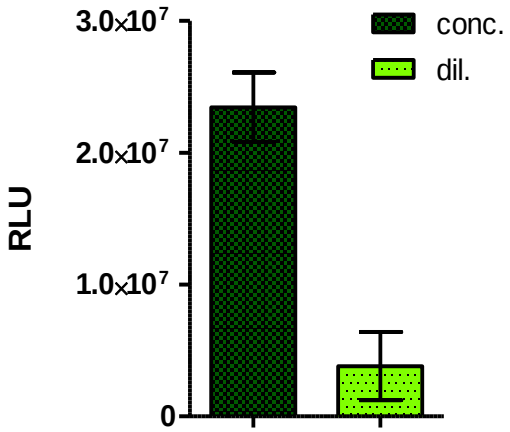

Fig. 46 - Increase in signal following the buffer exchange and protein concentration.

4.2.4 Luciferase characterization: bioluminescence emission kinetics and spectra

Bioluminescence emission kinetics (Fig. 47) and spectra (Fig. 48), obtained as described in the Materials and Methods section, for the purified protein were determined using LH_2 and Mg–ATP for green bioluminescent protein and using NanoGlo substrate for NanoLuc luciferase.

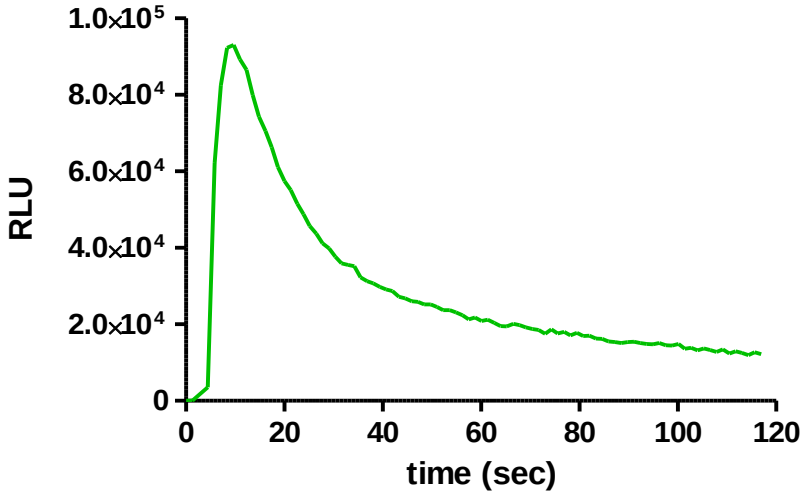

Fig. 47 - Bioluminescence time course of luciferase CUBOPT reaction.

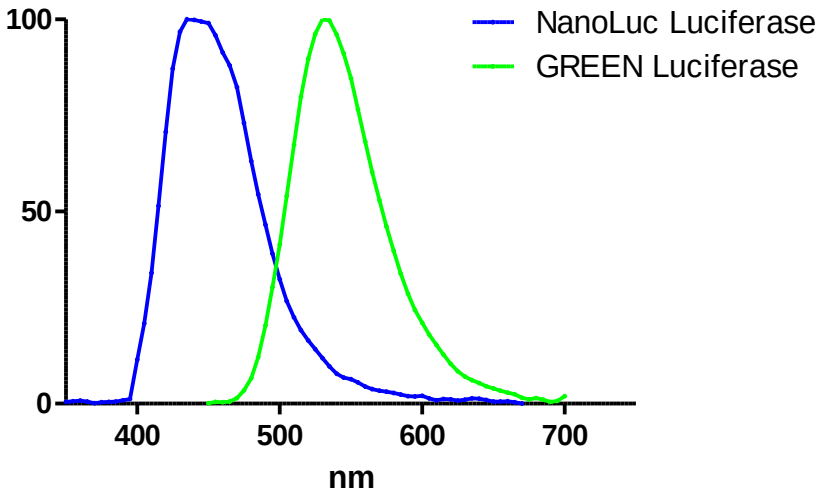

Fig. 48 – Emission spectra of NanoLuc luciferase and Green luciferase

The kinetic profile displays a flash emission typical of firefly luciferases with a peak after 10 sec and a signal half-life of 25 sec. The flash height-based measurements correspond to the maximum achievable overall reaction rate of light emission, a process dependent on the adenylation of substrate firefly luciferin followed by a multi-step oxidation of the intermediate to yield the light-emitting species oxyluciferin. Then, the signal remains stable at about a 25% of the highest value. The spectra of the in vitro purified proteins confirm that there is no spectral shift observed between the in vitro and in vivo BL emission, confirming the stabilizing effect of the luciferase.

4.2.5 NanoLuc luciferase emission in wells coated with different paints

The emission of NanoLuc luciferase was evaluated using different coatings; several materials for supporting printing, print density and waterproofing tops were evaluated as described in material and methods. An increase in the bioluminescent signal was reported between uncoated and coated well (Fig. 49). In particular, wells with coated white paint (white acrylic resin) showed a BL signal two times higher than those obtained with uncoated

well. Also, other paintings (i.e. yellow and orange fluorescent acrylic coatings) showed an increase of the signal.

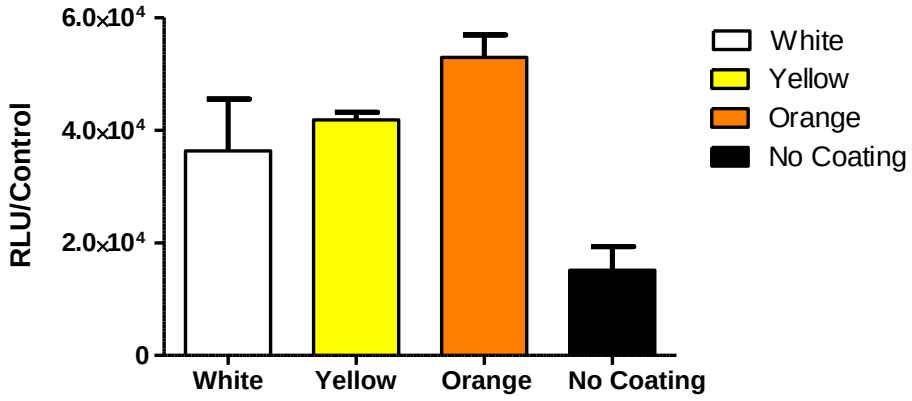

Fig. 49 - NanoLuc bioluminescent signal obtained with PLA well coated with different paint

Several dilutions were tested in order to evaluate the enhancer effect or the coating over different BL signal and protein concentration (Fig. 50).

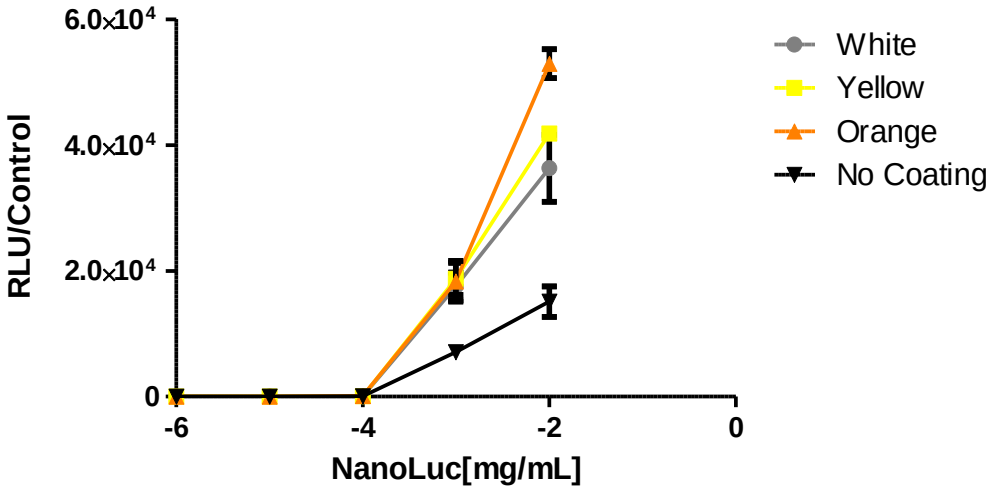

Fig. 50 Bioluminescent signal obtained with PLA well coated with different paint

As can be seen in the figure above, the enhancing effect of the painting influences all the tested concentrations. BL emission spectra of NanoLuc luciferase within the different

painted wells was acquired (Fig. 51). However these preliminary results require further investigations, in order to assess the actual feasibility of this approach.

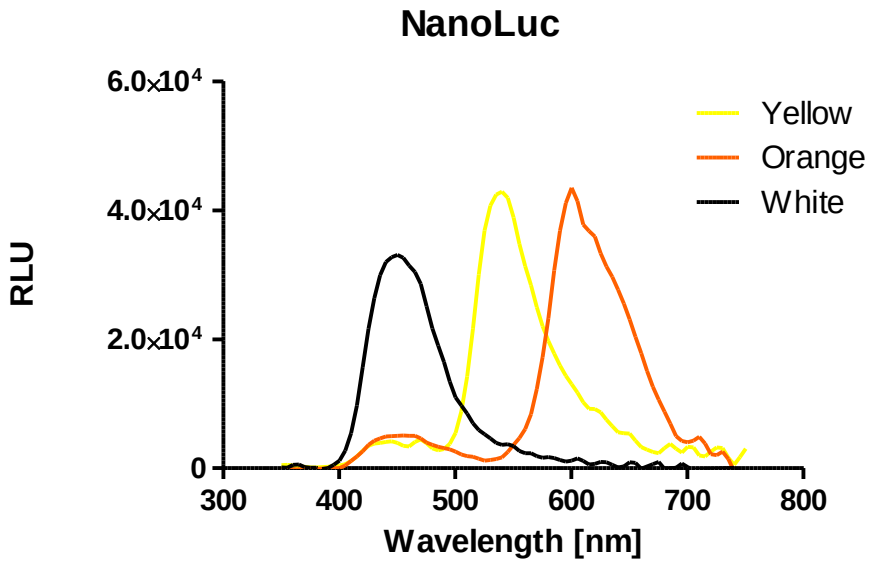

Fig. 51- NanoLuc bioluminescent spectra obtained with PLA well coated with different paints.

4.2.6 Analytical performance of the PpyGRT and NanoLuc purified proteins with portable light detectors

After the preliminary characterization of the PpyGRT and NanoLuc purified proteins, we optimized the assay conditions and evaluated its analytical performance by detecting BL signals of purified proteins in a dose-dependent manner. To this end, 5 µL-volumes of PpyGRT and NanoLuc solutions in the range of 10^{-6} - 10^{-10} M (1.0 x 10^{-1} - 1.0 x 10^{-6} mg/ml) were analyzed and BL signals were obtained after the addition of 10 µL of the substrate. BrightGlo substrate was used for PpyGRT luciferase and NanoGlo substrate was used for NanoLuc luciferase. The maximum performance settings of 5 min was employed for the SiPM detector.

In addition, for in-house comparison of the analytical performance of the SiPM detector, PpyGRT and Nanoluc proteins solutions were analyzed with a cooled CCD

camera (ATIK 383L), and OnePlus 6 smartphone camera, selected for their built-in ProCam application enabling manual selection of parameters including shutter-speed up to 30 sec and ISO settings values up to 3200 for low-light applications. The maximum performance settings of 30 sec with ISO 3200 for OnePlus 6 was employed for analyzing BL signals of PpyGRT and Nanoluc solutions. For the cooled CCD camera, the BL signals were acquired for 5 min at room temperature and at 5°C. The results are also compared with a conventional luminometer Varioskan Flash multimode reader.

Calibration curves for PpyGRT luciferase and NanoLuc luciferase are shown in Fig. 52. A LOD of 1.0 x 10^{-13} M and 1.0 x 10^{-14} M (6.0 x 10^{-8} mg/mL and 2.0 x 10^{-4} ng/mL) were obtained for PpyGRT and NanoLuc luciferases, respectively. Despite the Nanoluc luciferase is considered the brighter luciferase, a higher LOD was obtained with the Varioskan Flash multimode reader due to the flash kinetic emission properties.

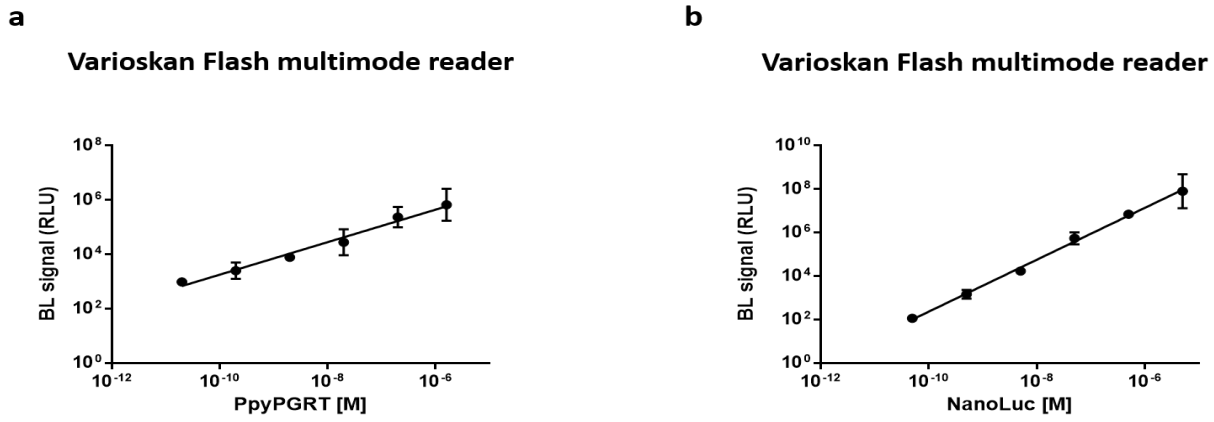

Fig. 52 - Calibration curves for PpyGRT luciferase and NanoLuc luciferase Values represent the average of 6 experiments ± SD.

The LODs for PpyPGRT and NanoLuc luciferases with a cooled CCD portable camera, were also investigated. By integrating the BL signals for 5 min at room temperature and at 5°C, for PpyGRT luciferase the same LODs of LODs of 3,3 x 10^{-8} M (2.0 x 10^{-3} mg/mL) were obtained using the ATIK 383L (Fig. 53).

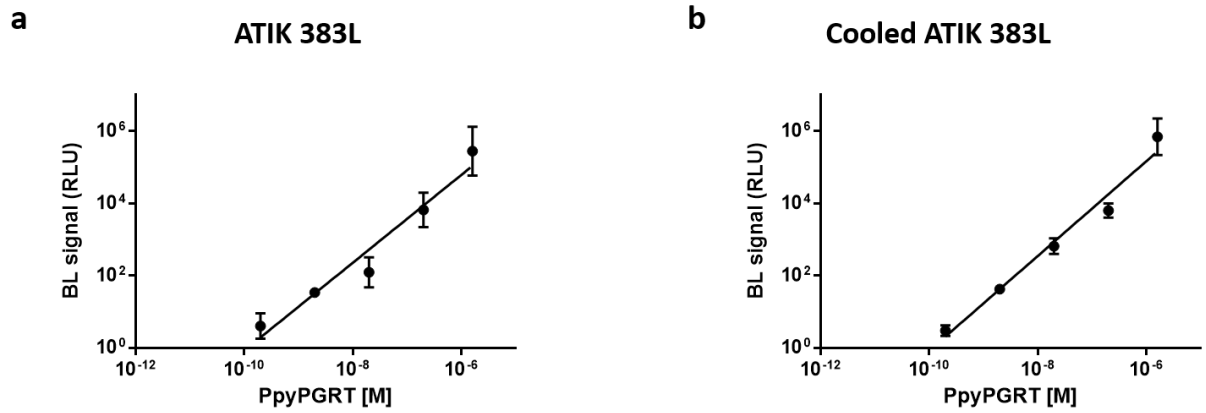

Fig. 53 - Calibration curves for PpyGRT luciferase protein obtained with a CCD camera, integrating BL signal for 5 min at room temperature (a) and at 5°C (b). Values represent the average of 6 experiments ± SD.

Concerning the analytical performance of SiPM detector, calibration curves of PpyPGRT luciferase was also obtained, integrating the BL signals for 5 min. All measurements were carried out at room temperature. As shown in Fig. 54, a LOD of LOD 1.7 x 10^{-8} M (1.0 x 10^{-3} mg/mL) was obtained for PpyPGRT luciferase, confirming the suitability of this not cooled SiPM sensor for bioluminescent analysis.

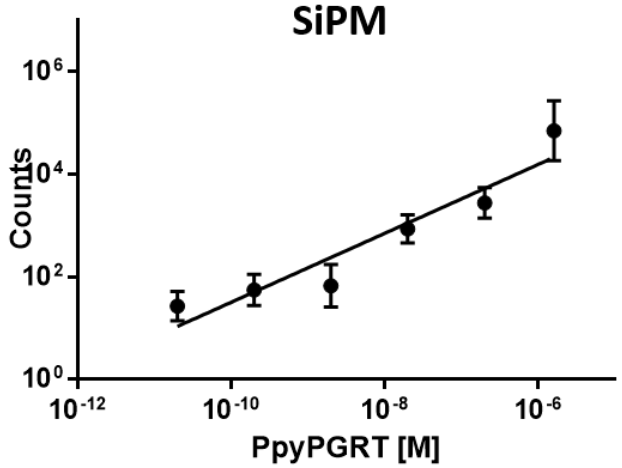

Fig. 54 -Calibration curve for PpyGRT luciferase protein obtained with a SiPM portable detector, integrating BL signal for 5 min at room temperature. Values represent the average of 6 experiments ± SD.

LODs of 9.5 x 10^{-8} M and 7,9 x 10^{-8} M (1.8 x 10-3 and 1.5 x 10-3 mg/mL) were obtained for NanoLuc luciferase with ATIK 383L at room temperature and at +5°C, respectively (Fig. 55).

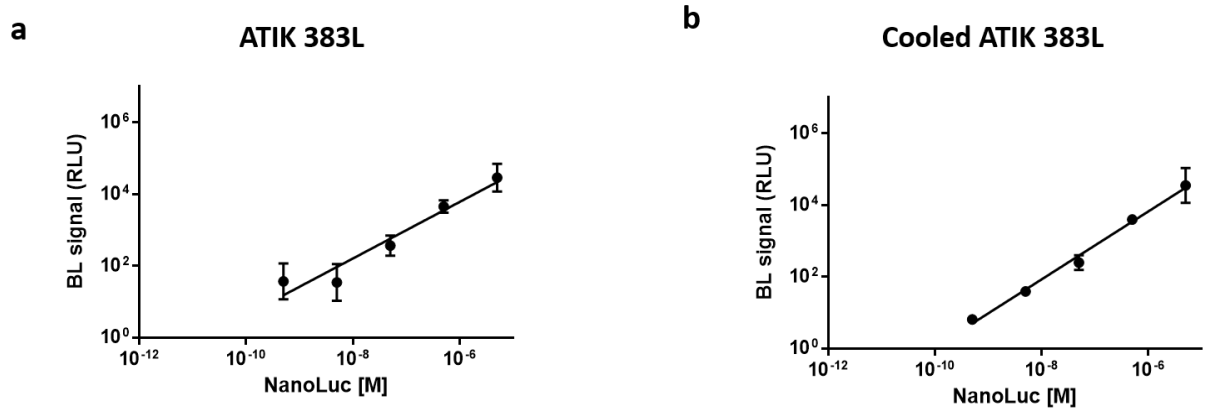

Fig. 55 - Calibration curves for NanoLuc luciferase protein obtained with a CCD camera, integrating BL signal for 5 min at room temperature (a) and at 5°C (b). V Values represent the average of 6 experiments ± SD.

The analytical performance of SiPM portable detector was also evaluated using the NanoLuc luciferase, obtaining a LOD of 5,3 x 10^{-9} M (1.0 x 10^{-4} mg/mL), one order of magnitude lower than those obtained with the ATIK 383L camera. This is due to the higher sensitivity of the sensor at the wavelengths in the blue emission spectra.

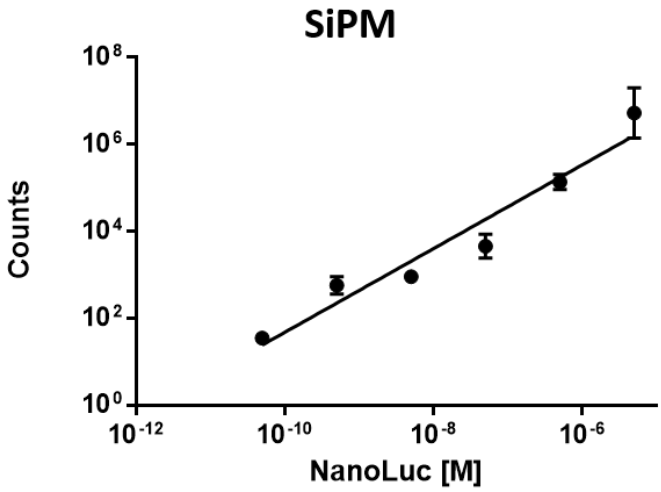

Fig. 56 - Calibration curve for NanoLuc luciferase protein obtained with a SiPM portable detector, integrating BL signal for 5 min at room temperature. Values represent the average of 6 experiments ± SD.

Under optimized conditions, the BL signal is proportional to the concentration of the luciferase showing a LOD of 1.7 x 10^{-6} M (0.1 mg/mL) for PpyGRT and LOD of 5.3 x 10^{-7} M (0.01 mg/mL) for Nanoluc luciferase with OnePlus 6 camera (Fig. 57).

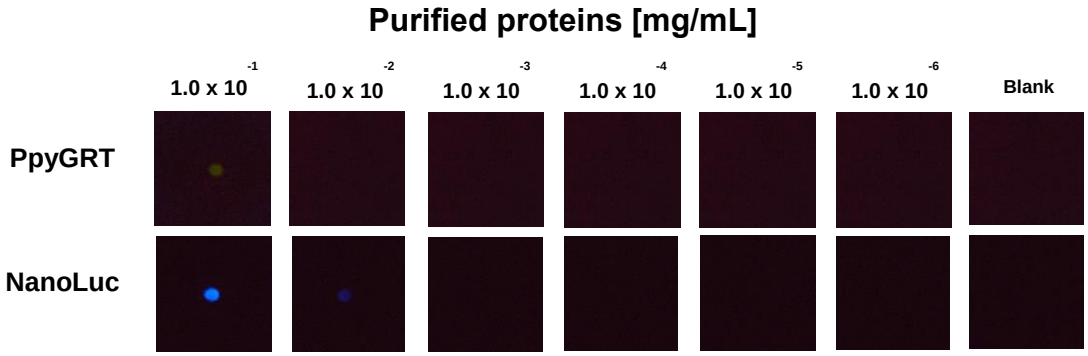

Fig. 57 - BL images of serial dilution of PpyGRT and NanoLuc luciferases obtained with OnePlus 6 smartphone at 3200 ISO setting and 30-s acquisition time.

Thanks to the significant improvement of the LODs, these results confirmed the suitability of SiPM for forensic applications such as for quantitative and rapid detection of nerve gases and pesticides. These results agree with the spectra sensitivity of this class of detector.

Chapter 5

Development of a proof-of-principle SiPM-based enzyme biosensor for chemiluminescence detection of nerve agents and pesticides

5.1 Materials and methods

5.1.1 Reagents

Acetylcholinesterase from *Electrophorus electricus* 100 U/mL (EC 3. 1. 1. 7), Choline Oxidase from Alcaligenes sp. 20 U/mL (EC 1. 1. 3. 17), HRP, Peroxidase Type VI-A from horseradish 108 U/mL (EC 1. 11. 1. 7), acetylcholine chloride 10 mM and luminol sodium salt were provided by Sigma Aldrich. A 0.025 M luminol solution in 0.1 M NaOH was used for the assay to maintain a basic enzyme-friendly environment and to exploit the improved properties of luminol in a basic environment.

Acetylcholinesterase is soluble in 20 mM Tris-HCl buffer pH 7.5 yielding a clear solution, stock solutions of 100 U/mL have been stored at - 20 °C. To obtain stock solutions of 20 U/mL, choline oxidase was solubilized in 10 mM Tris-HCl pH 8.0, with 2.0 mM EDTA and 134 mM KCl. Stock solutions of choline oxidase have been stored at - 20 °C. HRP was solubilized in 20 mM Tris-HCl pH 7.5. Chromatography paper Whatman 1 CHR (GE Healthcare, UK) was used for the Origami Paper-based Analytical Device (PAD).

5.1.2 Fabrication and assembling of the origami paper-based device

The origami PAD consists of 5 wells made with wax printing technique (Fig.58), performed with a Xerox ColorQube 8570DN printer simply connected with a USB cable to the computer to manage the operations to be performed. After having printed on the absorbent paper, a heating process was carried out with a heating plate at 100 °C for 30 seconds. Paper was brought closer to the heating plate so that the printed wax melted with heat and spread deep into the paper. This heating step is necessary to make the borders of the wells hydrophobic not only superficially but also in depth. PADs have been developed for a possible test to detect the presence of pesticides in a liquid sample, as can be the waters of rivers, lakes or groundwater. In well number 1, 5 µL of acetylcholinesterase were absorbed, in well number 2 and 3, 15 µL of choline oxidase were absorbed for a final. In well number 3 about 15 µL of HRP were absorbed. The pad was left to dry for 30 minutes at 37 °C. In the central well, 10 µL of final 10 mM Ach and 10 µL of water or sample must be added at the time of the test. These 20 µL correspond to the liquid phase that must wet the paper so that the enzymes absorbed in the wells are mixed and the reaction starts. The wells are numbered according to the order in which they are to be folded.

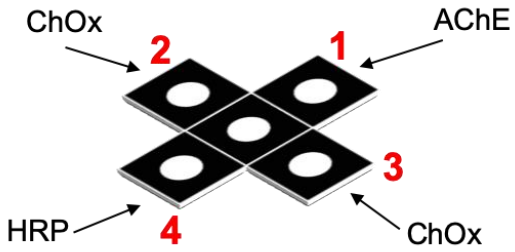

Fig 58 - Schematic representation of enzyme absorbed on PAD

5.1.3 Analytical procedure of the assay with the origami PAD

This assay is based on the inhibition of acetylcholinesterase by harmful molecules. For this reason, the control PAD corresponds to the total absence of organophosphorus compound, so the maximum activity of acetylcholinesterase, which appears as the maximum emission of light. As regards the analytical procedure (Fig. 59), firstly the sample was added to the well in which AChE had been absorbed. A 5-minute incubation was necessary and after the well number one was folded towards the central well and acetylcholine was added for co-incubation with AChE and sample. At this point the two lateral wells, where choline oxidase had been absorbed, were folded and again a 5-minute incubation was necessary to allow the formation of hydrogen peroxide which is inversely proportional to the concentration of the organophosphorus compound. In fact, only free active sites of AChE will produce choline which will subsequently be transformed into hydrogen peroxide by choline oxidase. At this point, once the incubation time was over, the well with absorbed peroxidase (HRP) was folded and luminol was added. The origami PAD was kept closed in a specific sample-holder, designed to firmly maintain it at about 1,5 mm from the SiPM sensor (Fig. 30, 32, 33). In the end, after 3 minutes of incubation the chemiluminescent signal was acquired for 5 minutes at room temperature with ArduSiPM photon detection system.

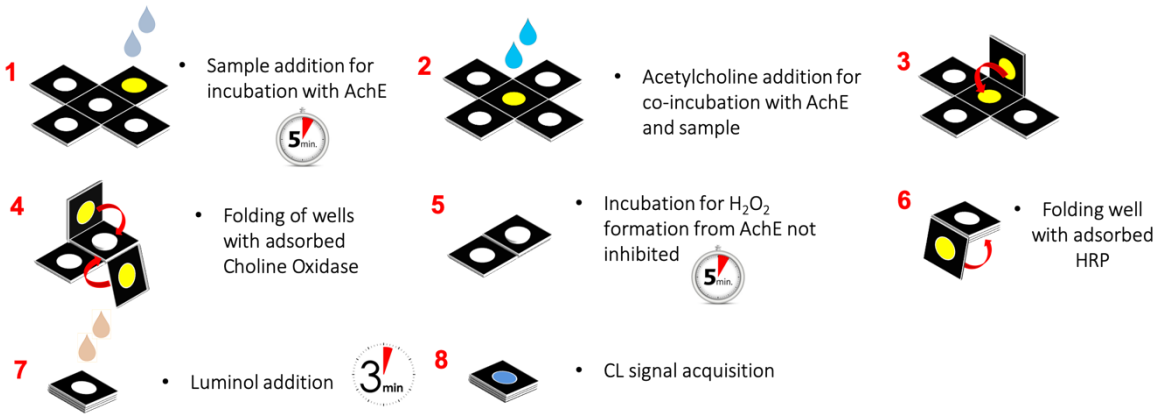

Fig 59 - schematic representation of the analytical procedure

5.2 Results and discussions

5.2.1 Simulated inhibition curve of acetylcholinesterase

As a proof of concept, a simulated acetylcholinesterase inhibition curve was performed to simulate the use of SiPM detection device. To simulate the inhibition of the enzyme acetylcholine esterase, decreasing concentrations of the latter have been absorbed on different PADs. A decrease in the active acetylcholinesterase corresponds to a greater concentration of organophosphorus compound which in turn corresponds to a lower chemiluminescent signal. Following the analytical procedure described above, decreasing concentrations of acetylcholine esterase were measured with the SiPM device. In the initial step, 10 uL of water was added instead of the sample. As shown in figure 60, decreasing concentrations of acetylcholinesterase absorbed on PAD corresponds to lower chemiluminescent intensities, which is related to an increased percentage of acetylcholinesterase inhibition. For this inhibition curve a LOD of 0.0002 U/mL of acetylcholinesterase was obtained, which corresponds to 90.7% of acetylcholinesterase inhibition.

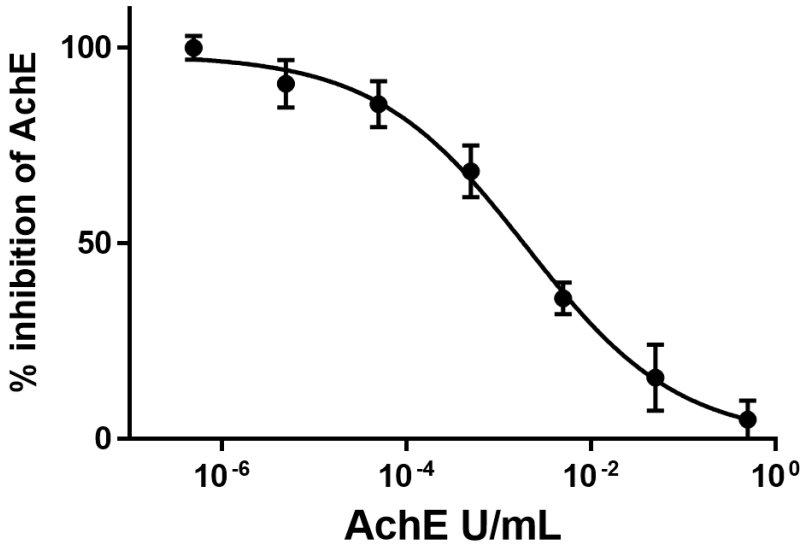

Fig. 60 - simulated acetylcholinesterase inhibition curve

Chapter 6

Conclusions

Real-time routine monitoring for chemical and biological threat agents is one of the major concerns of our society. A rapid response to a terrorist attack, as well as to an accidental release of toxic environmental pollutants, requires the ability to rapidly detect chemical and biological agents so that an early warning can be raised, potential health risks defined, and proper countermeasures are employed. The aim of this PhD research was thus focused on the development of a new portable analytical device for the detection of bio/chemiluminescence signals suitable for implementation by scientific police routine screenings and inspections.

The suitability of different portable light detectors was investigated, including CCDs and smartphone integrated CMOSs, and the Silicon Photomultiplier (SiPM) technology was selected for its main features, including high sensitivity, the requirement of very low voltage (few tens of volts), and use of discrete electronic circuits for fast signal acquisition. Such advantages enable the use of SiPM for the development of very compact and simple devices suitable for use in remotely controlled and totally standalone conditions.

In this research work, a SiPM detector, controlled by an ArduSiPM board, a specialized shield for Arduino DUE platform, was exploited to analyze bioluminescence and chemiluminescence reactions, in order to demonstrate its potential suitability as an

alternative to expensive bench-top instruments based on photomultiplier tubes and also to portable CCD and CMOS. Moreover, the small footprint, the lightness and the possibility of using it on batteries of ArduSiPM makes it really appealing for possible on-field uses.

The employed SiPM is based on a novel kind of G-APDs matrix, with “Reach-Through Epitaxial structure”, suitable for room temperature working activities, with acceptable noise figures. The detector spectral response peak is in the visible region, about at 450 nm; typical driving voltages are in the order of 50-60 V or less.

To use this sensor for low-light detection, a two-part black-box, named LuminoSiPM, was designed by a 3D CAD software (FreeCAD ver. 0.18) and fabricated in polylactic acid polymer by 3D printing. Interchangeable disposable sample-holders useful for liquid samples analysis and for the analysis of origami paper-based biosensors were 3D printed using a UV sensitive resin. Several parameters were optimized to reduce dark noise and improve signal to noise ratio. A comparison of the LuminoSiPM performance with benchtop instrumentation (Varioskan Flash), a cooled CCD (ATIK 383L), and OnePlus 6 smartphone integrated CMOS, was performed using solutions of two luciferases emitting at different wavelength. In particular two luciferases, a green-emitting P-pyralis mutant PpyGRT and the blue-emitting NanoLuc, were expressed in *E. coli* cells and purified. After the preliminary characterization of the PpyGRT and NanoLuc purified proteins, an in house comparison of different detectors was performed using PpyGRT and NanoLuc solutions (concentration range 10^{-6} - 10^{-10} mg/mL). A limit of detection (LOD) of 5.3×10^{-9} M was obtained with Nanoluc, about one order of magnitude lower than those obtained with the ATIK 383L camera. An higher LOD was obtained for PpyPGRT luciferase (1.7×10^{-8} M), most likely due to the lower sensitivity of the sensor at these wavelengths. In fact, sensitivity of the SiPM is optimal in the blue region of the visible spectrum, with a maximum corresponding to the emission peak of the Nanoluc (λ_{max} 490 nm), while it decreases of about 5% in the green region (λ_{max} of PpyGRT

550 nm). Lower performance was obtained with OnePlus 6 camera, that provided a LOD of 1.7×10^{-6} M for PpyGRT and 5.3×10^{-7} M for Nanoluc luciferase.

These positive results prompted the development of a proof-of-principle forensic application relying on a paper-based origami chemiluminescent biosensor for rapid detection of nerve gases and pesticides. This biosensor is based on the inhibition process of acetylcholinesterase (AChE) by molecules such as organophosphate pesticides, nerve gases and some drugs. The AChE activity is measured through a series of coupled enzymatic reactions leading to light emission. When acetylcholinesterase is inhibited, there is a decreased production of hydrogen peroxide, and consequently a reduction in light emission. In particular, three different enzymes, AChE, choline oxidase (ChOx) and Horse Radish Peroxidase (HRP), are adsorbed on a paper pad obtained by wax printing. The origami technique allows to add reagents in separate steps and trigger the reactions to occur sequentially.

A simulated acetylcholinesterase inhibition curve was performed to simulate the use of SiPM detection device. A LOD of 0.0002 U/mL of acetylcholinesterase was obtained, corresponding to 90.7% of acetylcholinesterase inhibition. These encouraging results provide the proof-of-concept feasibility of implementing the LuminoSiPM device to detect low light of bioluminescence and chemiluminescence biosensors in criminal investigations and other forensic-related activities. Nevertheless, further improvements, such as cooling of the sensor, temperature control of the device, ability to measure fast light emission signal kinetics will be required to improve the limits of detection for applications in real settings and the device robustness.

SiPM outlook in forensic sciences

SiPM sensors appear particularly eligible for portable instruments designed for law-enforcement and, more in general, for on-field forensic analysis. They have a solid-state, rugged constitution, can express PMT range sensitivities, ensuring long and continuous periods thanks to operative low tensions and minimal energy consumptions. Moreover they are easily configurable in stand-alone or remote-controlled operative mode, especially requested in dangerous situations. Searching a possible weakness, a single SiPM lacks of imaging features, which are especially useful in criminal trials (visual evidence).

One of the most relevant application in security is the detection and identification of explosives in activities aimed at prevention of terrorism acts. In recent years, several analytical methods, based on luminescent reactions, have been developed to explosives' detection, as Chemiluminescent Enzyme-Linked Immunosorbent Assay (CL-ELISA) and Chemiluminescent Latelar Flow ImmunoAssay (CL-LFIA) methods (Girotti S. et al (2010, 2011), useful for peroxide or nitro aromatic-based energetic materials individuation (Romolo F.S. et al. 2015). For suitable on-field detection of faint photonic signals, were especially employed portable thermoelectrically cooled cameras, which have high sensitivity figures and enhanced imaging capabilities. Ne**v**ertheless, these apparatus are not properly miniaturisable, require external control units to collect experimental data.

Confirming the need to have sensitive and portable tools in critical security activities, commercial portable luminometers, originally designed to assess the level of cleanliness of surfaces and materials in healthcare and environmental control, have been proposed to locate improvised explosive manufacturing sites, where is employed hydrogen peroxide (Romolo F.S. et al. 2016). It is necessary to note that these instruments, although based on sensitive photodiodes, need to balance the absence of internal amplification (photodiode

gain=1) with an accurate design of sampling tools (e.g. kit for ATP or bacterial monitoring), not specifically intended for other finalities, such as continuous operational tasks.

However, forensic applications of SiPM sensors might noticeably increase in the near future, considering recent studies on digital versions of this technology (dSiPM). In contrast to conventional SiPM, where SPAD cells, by means of passive component (e.g. quenching resistors), work all together in parallel, generating an unique “analogic” signal, which is affected by several interferences and need for a further AC/DC conversion, in dSiPM the conjunction of well-established digital CMOS technology with SPAD permit to integrate active quenching, recharge and digital readout circuitry directly in all cell of matrix. In this manner, the sensor can be driven at single-cell-level and, considering that every phase of signal readout (in/out) happen in the digital domain, noise and interferences sources can be largely reduced (Schaart D. R. et al. (2016)).

At present, this innovative technology is mainly employed in several fields of medical research (e.g. positron emission tomography, PET). However, considering the possibility to control independently each single cell of sensor, it is predictable that, with appropriate granularities of matrix, it will be possible to implement imaging features, even in single sensor configurations. In this way, this totally digital version might combine to the ultra-sensitivity of SiPMs the main advantage of imaging matrix detectors.

References

1. Andreescu S., Marty J.L., “Twenty years research in cholinesterase biosensors: From basic research to practical applications”. Biomolecular Engineering, 2006; 23: 1-15.
2. Bhagavan N.V., Ha C.E., “Enzymes and enzyme Regulation”. Essentials of Medical Biochemistry, 2011. Chapter 6: 47-58.
3. Bondarenko G et al 2000 “Limited Geiger-mode microcell silicon photodiode: new results”, Nucl. Instrum. Methods Phys. Res. A 442 187– 92.
4. Bruzewicz D. A., Reches M., Whitesides G. M., “Low-cost printing of poly(dimethylsiloxane) barriers to define microchannels in paper”. Anal. Chem., 2008; 80, 3387–3392.
5. Buzhan, P., Dolgoshein, B., Filatov, L., Ilyin, A., Kantzerov, V., Kaplin, V., Karakash, A.,Kayumov, F., Klemin, S., Popova, E., Smirnov, S., 2003. Nucl. Instrum. Methods Phys. Res. Sect. A-Accel. Spectrom. Dect. Assoc. Equip. 504 (1–3), 48–52.
6. Carrilho E., Martinez A. W., Whitesides G. M., “Understanding Wax Printing: A Simple Micropatterning Process for Paper-Based Microfluidics”. Anal. Chem., 2009, 81, 7091–7095.
7. Cate D. M., Adkins J. A., Mettakoonpitak J., Henry Ch. S., “Recent developments in paper-based microfluidic devices”. Anal. Chem., 2015; 87: 19–41.
8. Christensen DA, Herron JN. Methods Mol Biol. 2009;503:239-58. Optical system design for biosensors based on CCD detection.
9. Cunningham J. C., Scida K., Kogan M. R., Wang B., Ellington A. D., Crooks R. M., “Paper diagnostic device for quantitative electrochemical detection of ricin at picomolar levels”. Lab Chip, 2015, 15, 3707–3715.
10. Dai, Z.; Xu, L.; Duan, G.; Li, T.; Zhang, H.; Li, Y.; Wang, Y.; Wang, Y.; Cai, W. IEEE Photonics Technology Letters 2019 vol:31 iss:20 pg:1619 -1622
11. Damulira, E., Yusoff, M.N.S., Omar, A.F., Taib, N.H.M. A review: Photonic devices used for dosimetry in medical radiation (2019) Sensors (Switzerland), 19(10),2226
12. Delaney J. L., Hogan C. F., Tian J., Shen W., “Electrogenerated chemiluminescence detection in paper-based microfluidic sensors”. Anal. Chem., 2011, 83, 1300–1306.
13. Dolgoshein, B., Balagura, V., Buzhan, P., Danilov, M., Filatov, L., Garutti, E., Groll, M., Ilyin, A., Kantserov, V., Kaplin, V., Karakash, A., Kayumov, F., Klemin, S., Korbel, V., Meyer, H., Mizuk, R., Morgunov, V., Novikov, E., Pakhlov, P., Popova, E., Rusinov, V., Sefkow, F., Tarkovsky, E., Tikhomirov, I., 2006. Nucl. Instrum. Methods Phys. Res. Sect. A-Accel. Spectrom. Dect. Assoc. Equip. 563 (2),368–376.
14. Eltzov E., Cohen A., Marks R. S., “Bioluminescent Liquid Light Guide Pad Biosensor for Indoor Air Toxicity Monitoring”. Anal. Chem. 2015; 87: 3655-3661.
15. Engelking L.R., “Enzyme Kinetics”. Textbook of Veterinary Physiological Chemistry, 2015; Chapter 6: 32-38.
16. Fitch JP, Raber E, Imbro DR. Technology challenges in responding to biological or chemical attacks in the civilian sector. Science. 2003 Nov 21;302(5649):1350-4.

17. Ge L., Wang S., Song X., Ge S., Yu J. “3D Origami-based multifunction-integrated immunodevice: low-cost and multiplexed sandwich chemiluminescence immunoassay on microfluidic paper-based analytical device”. Lab Chip, 2012; 12, 3150-3158.
18. Graham Davies, R.;, J.; Canepari, M. Light sources and cameras for standard in vitro membrane potential and high-speed ion imaging (2013) J Microscopy, 251, 5-13
19. Guardigli M., Pasini P., Mirasoli M. Leoini A., Andreani A, Roda A. “Chemiluminescent high-throughput microassay for evaluation of acetylcholinesterase inhibitors”. Analytica Chimica Acta, 2005; 535: 139-144.
20. H. Cansizoglu et al., "Dramatically Enhanced Efficiency in Ultra-Fast Silicon MSM Photodiodes Via Light Trapping Structures," in IEEE Photonics Technology Letters, vol. 31, no. 20, pp. 1619-1622, 15 Oct.15, 2019.
21. He Y., Wu Y., Fu J.-Z., Wu W.-B., “Fabrication of paper-based microfluidic analysis devices: a review”. RSC Adv., 2015; 5, 78109–78127.
22. Hu J., Wang S. Q., Wang L., Li F., Pingguan-Murphy B., Lu T. J., Xu F., “Advances in paper-based point-of-care diagnostics”. Biosens. Bioelectron., 2014; 54:585–597.
23. INAF web Publication https://www.media.inaf.it/2019/06/05/hamamatsu-astri/
24. J.H. Kim, H.M. Park and K.S. Joo “Development of compact and real-time radiation detector based on SiPM for gamma-ray spectroscopy”, Journal of Instrumentation, Volume 13, July 2018
25. Li H, Lopes N, Moser S, Sayler G, Ripp S (2012) Silicon photomultiplier (SPM) detection of low-level bioluminescence for the development of deployable whole-cell biosensors: possibilities and limitations. Biosens Bioelectron. 2012 Mar 15;33(1):299-303.
26. López-Marzo A.M., Merkoçi A. “Paper-based sensors and assays: a success of the engineering design and the convergence of knowledge areas”. Lab Chip, 2016; 16: 3150-3170.
27. Lu Y., Shi W., Jiang L., Qin J., Lin B., “Rapid prototyping of paper-based microfluidics with wax for low-cost, portable bioassay”. Electrophoresis, 2009; 30, 1497–1500.
28. Martinez A. W., Phillips S. T., Whitesides G. M., “Diagnostics for the developing world: microfluidic paper-based analytical devices”. Anal. Chem., 2010; 82: 3–10.
29. Mirasoli M., Guardigli M., Michelini E., Roda A. “Recents advancements in chemical luminescence-based lab-on-chip and microfluidic platforms for bioanalysis”. J Pharmaceut Biomed, 2014; 87: 36-52.
30. Morales-Narváez E., Naghdi T., Zor E., Merkoçi A., “Photoluminescent Lateral-Flow Immunoassay Revealed by Graphene Oxide: Highly Sensitive Paper-Based Pathogen Detection”. Anal. Chem., 2015, 87, 8573–8577.
31. Nath P., Arun R. K., Chanda N., “Smart gold nanosensor for easy sensing of lead and copper ions in solution and using paper strips”. RSC Adv., 2015; 5, 69024–69031.
32. Norian, H.; Field, R.M.; Kymissis, I.; Shepard, K.L. An integrated CMOS quantitative-polymerase-chain reaction lab-on-chip for point-of-care diagnostics. Lab Chip 2014, 14, 4076–4084.
33. Pasini P., Musiani M., Russo C., Valenti P., Aicardi G., Crabtree J.E., Baraldini M., Roda A. “Chemiluminescent imaging in bioanalysis”. Journal of Pharmaceutical and Biomedical Analysis, 1998; 18: 555-564.
34. Pires, N.M.M.; Dong, T.; Hanke, U.; Hoivik, N. Recent developments in optical detection technologies in lab-on-a-chip devices for biosensing applications. Sensors 2014, 14, 15458–15479.

35. Pundir C.S., Chauhan N., “Acetylcholinesterase inhibition-based biosensors for pesticide determination: A review”. Analytical Biochemistry, 2012; 429: 19-31.
36. Roda A., Mirasoli M., Michelini E., Di Fusco M., Zangheri M., Cevenini L., Roda B., Simoni P. “Progress in chemical luminescence-based biosensors: a critical review”. Biosensors and Bioelectronics, 2016; 76, 164-179.
37. Roda A., Pasini P., Guardigli M., Baraldini M., Musiani M., Mirasoli M. “Bio- and chemiluminescence in bioanalysis”. Fresenius J Anal Chem, 2000; 366, 752-759.
38. Ryan D. Sochol, Eric Sweet, Casey C. Glick, Sung-Yueh Wu, Chen Yang, Michael Restaino, Liwei Lin, 3D printed microfluidics and microelectronics, Microelectronic Engineering (2018) 189, 52-68
39. Sadik OA, Wanekaya AK, Andreescu S. Advances in analytical technologies for environmental protection and public safety. J Environ Monit. 2004 Jun;6(6):513-22.
40. Samuela Lomazzi et al. “A SiPM based novel approach to cytosolic calcium detection bybioluminescence” - SiPM Workshop: from fundamental research to industrial applications 4th October 2019 – Bari.
41. Schöning M. J., Krause R., Block K., MusahmehnM., Mulchandani A., Wang J. “A dual amperometric/potentiometric FIA-based biosensor for the distinctive detection of organophosphorus pesticides”. Sensors and Actuators B: Chemical, 2003; 95: 291-296.
42. Singh S. Sensors--an effective approach for the detection of explosives. J Hazard Mater. 2007 Jun 1;144(1-2):15-28.
43. Songa E.A., Okonkwo J.O. “Recent approaches to improving selectivity and sensitivity of enzyme-based biosensors for organophosphorus pesticides: A review”. Talanta, 2016; 155, 289-304.
44. Sun G., Liu H., Zhang Y., Yu J., Yan M., Songand X., He W., “Gold nanorods-paper electrode-based enzyme-free electrochemical immunoassay for prostate specific antigen using porous zinc oxide spheres–silver nanoparticles nanocomposites as labels”. New J. Chem., 2015, 39, 6062–6067.
45. Sun G., Wang P., Ge S., Ge L., Yu J., Yan M., “Photoelectrochemical sensor for pentachlorophenol on microfluidic paper-based analytical device based on the molecular imprinting technique”. Biosens. Bioelectron., 2014; 56, 97–103.
46. T. Maruhashi et al “Evaluation of a novel photon-counting CT system using a 16-channel MPPC array for multicolor 3-D imaging”, Nuclear Inst. and Methods in Physics Research, A 936 (2019) 5–9
47. Tang D., Sauceda J. C., Lin Z., Basova S., Goryacheva I., Biselli S., Lin J., Niessner R., Knopp D., “Magnetic nanogold microspheres-based lateral-flow immunodipstick for rapid detection of aflatoxin B2 in food”. Biosens. Bioelectron., 2009; 25, 514–518.
48. Tuan D. Ngo, Alireza Kashani, Gabriele Imbalzano, Kate T.Q. Nguyen, David Hui, Additive manufacturing (3D printing): A review of materials, methods, applications and challenges, Composites Part B: Engineering (2018) 143,172-196
49. U. Green, J.H. Kremer, M. Zillmer, C. Moldaenke, Detection of chemical threat agents in drinking water by an early warning real-time biomonitor, Environ.Toxicol. 18 (2003) 368–374.
50. V. Bocci et al. “The ArduSiPM a compact transportable Software/Hardware Data Acquisition system for SiPM detector”, 2014 IEEE Nuclear Science Symposium and Medical Imaging Conference (NSS/MIC); DOI: 10.1109/NSSMIC.2014.7431252.
51. Velu R., Frost N., DeRosa M. C., “Linkage inversion assembled nano-aptasensors (LIANAs) for turn-on fluorescence detection”. Chem. Commun., 2015, 51, 14346–14349.

52. Wang J., Krause R., Block K., Musameh M., Mulchandani A., Schöning M. J. “Flow injection amperometric detection of OP nerve agents based on an organophosphorus-hydrolase biosensor detector”. Biosensors and Bioelectronics, 2003; 18: 255-260.

53. Wang J., Monton M. R. N., Zhang X., Filipe C. D. M., Pelton R., Brennan J. D., “Hydrophobic sol–gel channel patterning strategies for paper-based microfluidics”. Lab Chip, 2014; 14, 691–695.

54. Wang S., Ge L., Song X., Yu J., Ge S., Huang J., Zeng F., “Paper-based chemiluminescence ELISA: lab-on-paper based on chitosan modified paper device and wax-screen-printing”. Biosens. Bioelectron., 2012; 31, 212–218.

55. Xia Y., Si J., Li Z., “Fabrication techniques for microfluidic paper-based analytical devices and their applications for biological testing: A review”. Biosens. Bioelectron., 2016, 77, 774–789.

56. Yi, X; Xie, SY; Liang, BL ; Lim, LW; Cheong, JS; Debnath, MC; Huffaker, DL ; Tan, CH ; David, JPR Extremely low excess noise and high sensitivity AlAs0.56Sb0.44 avalanche photodiodes (2019) Nature Photonics, 13, 683-693.

57. Zangheri M., Di Nardo F., Anfossi L., Giovannoli C., Baggiani C., Roda A., Mirasoli M., “A multiplex chemiluminescent biosensor for type B-fumonisins and aflatoxin B1 quantitative detection in maize flour”. Analyst, 2015; 140, 358-365.

58. Zhou F., Noor M. O., Krull U. J., “Luminescence Resonance Energy Transfer-Based Nucleic Acid Hybridization Assay on Cellulose Paper with Upconverting Phosphor as Donors”. Anal. Chem., 2014, 86, 2719–2726.

59. Girotti S., Eremin S., Montoya A., Moreno MJ, Caputo P., D’Elia M., Ripani L.,. Romolo F.S., Maiolini E., “Development of a chemiluminescent ELISA and a colloidal gold-based LFIA for TNT detection”. Anal. Bioanal Chem chemistry 2010 Jan;396(2):687-95.

60. Girotti S., Ferri E., Maiolini E., Bolelli L., D'Elia M., Coppe D., Romolo F.S., “A quantitative chemiluminescent assay for analysis of peroxide-based explosives”. Anal Bioanal Chem. 2011 Apr;400 (2):313-20.

61. Romolo F.S., Ferri E., Mirasoli M., D'Elia M., Ripani L., Peluso G., Risoluti R., Maiolini E., Girotti S., “Field detection capability of immunochemical assays during criminal investigations involving the use of TNT”. Forensic Sci Int. 2015 Jan;246:25-30.

62. Romolo F.S., Connell S., Ferrari C., Suarez G., Sauvain J-J., Hopf N.B., “Locating bomb factories by detecting hydrogen peroxide”, Talanta,160 (2016)15–20.

63. Schaart D. R., Charbon E., Frach T., Schulz V., “Advances in digital SiPMs and their application in biomedical imaging” Nuclear Instr. and Meth. in Physics Research A, 809 (2016), 31–52.

Acknowledgments

I would like to thank my Supervisor Prof. Aldo Roda for its belief in the possibility of realize this doctorate work in his research group and encouraged me to . An especial thanks go to co-Supervisors Prof. Elisa Michelini, who always expressed a great effort in support my activities, answering rapidly to all my questions and steering the research strategy. A great thanks goes to PhD Maria Maddalena Calabretta, who, ever with optimism in final results, gave me a great help in analytical activities.

A special mention goes to my adventure companions, Antonia Lopreside and Laura Montali, who helped me, sharing their precious experiences.

I want to thank my work colleague, Fabio Fragapane, for our lively discussions on practical Arduino platform applications and 3D printing technology, and my brother, Antonio, who provided me initial equipment, needed to test prototypal devices.

Finally, I must greatly to thank my darling family, that firmly sustained my work during all these years, despite the large amount of time spent on this mission.

.